



Recent advances in single-atom electrocatalysts supported on two-dimensional materials for oxygen evolution reaction

Journal:	<i>Journal of Materials Chemistry A</i>
Manuscript ID	TA-REV-01-2021-000154.R1
Article Type:	Review Article
Date Submitted by the Author:	08-Mar-2021
Complete List of Authors:	Zhou, Yanan; Sichuan University, School of Chemical Engineering; Lawrence Berkeley National Laboratory, Materials Science Division Li, Jing; Sichuan University (Top 12th Univ in China), Dept Chemical Engineering Gao, Xiaoping; Shanghai Jiao Tong University, School of Environmental Science and Engineering Chu, Wei; Sichuan University (Top 12th Univ in China), Dept Chemical Engineering Gao, Guoping; Lawrence Berkeley National Laboratory, Berkeley, Wang, Lin-Wang; Lawrence Berkeley National Laboratory,

Recent advances in single-atom electrocatalysts supported on two-dimensional materials for oxygen evolution reaction

Yanan Zhou,^{#a,b} Jing Li,^{#a} Xiaoping Gao,^{#c} Wei Chu,^{*a} Guoping Gao,^{*b} and Lin-Wang Wang^{*b}

^a School of Chemical Engineering, Sichuan University, Chengdu, 610065, Sichuan, China

^b Materials Science Division, Lawrence Berkeley National Laboratory, Berkeley, 94720, California, United States

^c School of Environmental Science and Engineering, Shanghai Jiao Tong University, Shanghai, 200240, China

*Corresponding authors.

These authors contributed equally to this work.

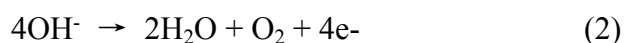
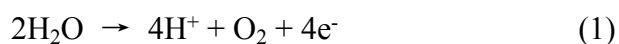
E-mail address: chuwei1965@scu.edu.cn (Wei Chu); ggao@lbl.gov (Guoping Gao); lwwang@lbl.gov (Lin-Wang Wang).

Abstract: As a half-reaction of electrolytic water-splitting for hydrogen generation, the oxygen evolution reaction (OER) is the major bottleneck due to its sluggish kinetics of the four-electron transfer reactions. Developing high-efficiency and cost-effective OER electrocatalysts are crucial to the advance of water-splitting. Besides the conventional metal-based nanoparticle catalysts, constructing single-atom catalysts (SACs) on two-dimensional (2D) materials has become an important research direction in recent years. In this review, we summarize the recent strategies to synthesis SACs, the experimental and theoretical studies of 2D materials-based SACs to enhance OER

performance, the rational design principles of SACs toward OER, as well as the challenges and future directions. A discussion is provided for a better understanding of OER, to guide the optimization of electrocatalysts, and for possible future candidates of SACs.

1. Introduction

To solve the global environmental crises caused by the fossil fuels consumption, great efforts have been made in the development of clean and sustainable energy in chemistry and materials science [1, 2]. Hydrogen is a promising clean energy storage medium due to its high energy density, environmental friendliness, and the harmless end by-product of water from its consumption [3, 4]. In particular, electrochemical water-splitting is recognized as one of the most promising technologies to produce hydrogen due to its safety, high efficiency, and pollution-free benign natures [5]. Electrochemical water-splitting comprises two half-reactions which are separated by a membrane [6]. The hydrogen evolution reaction (HER) at the cathode side and the oxygen evolution reaction (OER) at the anode side, corresponding to a reduction reaction and oxidation reaction, respectively. The thermodynamic potential of electrochemical water-splitting reaction is 1.23 V vs reversible hydrogen electrode (RHE) [7, 8]. As a half-cell reaction of electrochemical water-splitting at the anode, the four-electron transfer reaction of OER is the reaction bottleneck (compared with the two-electron transfer reaction of HER) due to its kinetic sluggishness. Therefore, the OER is the main research topic in many water-splitting studies. Under acidic and alkaline conditions, the overall OER can be described by the following equation (1) and (2), respectively [9, 10]:



Designing OER electrocatalysts for performance improvement is crucial for commercializing water-splitting process. Due to the availability of proton exchange membrane like Nafion, the commercial water-splitting systems are often under acidic condition. Currently, noble metal oxides IrO_2 and RuO_2 have been the state-of-the-art OER electrocatalysts in acidic condition [11-13]. However, the scarcity and high costs of

these noble-metals severely hinder their broad adoptions in the commercial water-splitting electrolyzers. The poor stabilities of IrO₂ and RuO₂ in strong alkaline solutions make them not suitable for high pH value situation [14-17]. In strong alkaline solutions, people have used Co₃O₄ [18] and NiFe-LDH (layered double hydroxide) [5] as the OER electrocatalysts. It is imperative to further design and develop cost-effective and stable electrocatalysts that can reduce the kinetic barrier and improve the efficiency of OER, preferably under both acidic and alkaline conditions.

Currently, there are two approaches to develop the desirable electrocatalysts especially to reduce its cost. One approach is to use less of the noble metals without decreasing the catalytic efficiency of the OER, the other is to develop nonprecious metal alternatives. In general, during catalysis, only the atoms on the surface of the catalytic materials are accessible to reactants and intermediate states [19]. Thus, for a bulk catalytic material, only a small portion of the metal species takes part in the catalytic reaction. Hence, reducing the metal particle sizes into small clusters can significantly increase the surface to bulk ratio, and has been proved to increase the catalytic efficiency [20, 21]. The ultimate version of such particle size reduction scheme is to disperse individual catalytic atoms on a substrate. Each catalytic atom will perform the catalytic function, serves as a single-atom catalyst (SAC) center. High utilization of the active atomic, uniform active center, low atomic coordination number at the active center, and high reaction selectivity are often the characteristics of SACs. Moreover, the relatively simple environments in SACs make them ideal systems to understand the catalytic mechanisms from both theoretical and experimental perspectives. Such understanding can further help us to design new SAC systems. In contrast, the conventional heterogeneous catalysis are often complicated by the existences of surface steps and corners, and the possibility of multiple binding sites. The understanding of SACs can rival that of the molecular homogeneous catalysis, which are however difficult to be used for electrochemistry. It is noteworthy that the per atom particle free energy increases with the reduction of the metal particle sizes. The isolated metal atoms can hardly exist alone and tend to aggregate to form metal clusters or nanoparticles. Therefore, it is essential to prevent the aggregation of these individually dispersed metal

atoms and maintain their stabilities via appropriate metal-substrate binding. Such binding strengths and coordination can also influence the catalytic properties of the SACs. Among various types of supports, many two-dimensional (2D) materials have been successfully used to form such SACs [22-25]. These include graphene, LDH, exfoliated graphitic carbon nitride, transition metal dichalcogenides (TMDs), MXene, layered metal-organic frameworks (MOFs) and covalent organic frameworks (COFs) [26, 27]. In general, the following properties of 2D materials have been taken advantage of as the supports of SACs: 1) Compared with their bulk counterparts, 2D materials feature with ordered layered atomic structure, possess stronger in-plane chemical bonding than out-of-plane interactions, exhibit enhanced charge mobility [24, 28] and large surface area; 2) 2D materials with open double-sided surfaces possess high percentage of exposed surface atoms that can easily escape from the respective lattice to form surface defects, which provides a large number of anchoring sites for the metal atoms [29]; 3) The uniformly exposed 2D layer and smaller electronic density of state of the 2D materials, make it more accessible for metal-substrate binding tuning through various ways, such as doping, alloying, and chemical functionalization [30], compared with the 3D structure counterparts; 4) In theory, 2D materials are simple computational models to understand the relationship between the structural properties and catalytic performance; in experiments, the synthesis and the techniques for characterization of 2D catalysts are being rapidly developed. Thus, using 2D materials as the supports of SACs provide researchers an excellent platform to deep understand the real atomic structure of active centers by combining experimental observations and theoretical simulations [31]. Nevertheless, the current investigation of the 2D material-based SAC (2D-SAC) for OER is still in its early stage. New insight and guidance for the design and optimization of 2D-SACs are urgently needed.

To date, many excellent reviews on the synthetic strategies, mechanism, and applications of single-atom catalysts on electrochemical water-splitting have been published [19, 32-34]. However, a detailed review concerning various types of 2D-SACs for electrochemical OER, in particular, related to advanced synthetic methods, a deep insight into the reaction mechanism, and the structure-activity relations will still be a

welcome addition to the literature. In this short review, we systemically summarize the recent theoretical and experimental progresses in 2D-SACs for OER. Firstly, we summarize the recent synthesis techniques for various 2D-SACs with an emphasis in comparing the advantages and disadvantages of different methods. Second, we highlight the electrochemical OER performances of various 2D-SACs and look into their structure-activity relationship. Third, we describe the detailed mechanisms of OER and the recent advances of using density functional theory (DFT) calculations for understanding the OER reaction steps. We show how such DFT calculation results can be used to rationally design the 2D-SACs for better OER performance. Finally, we discuss the current challenges, future opportunities, and possible research directions for using 2D-SACs for better OER performance. We hope our review can inspire future researches in this fast developing field.

2. Synthesis of 2D materials-based SACs

In essence, the synthesis of 2D-SAC materials involves either chemical (chemical reaction) or physical (sound, light, heat, electricity, magnetism, and force) process. Here, we briefly review the synthetically strategies of SACs, with a focus on their general aspects and fundamental insights.

2.1 Wet-chemical strategy

Broadly speaking, methods of material synthesis through wet-chemistry reaction can be divided into chemical reduction, electrochemical deposition, and photochemical reaction. The relatively easy operation and mild reaction conditions are the merits of the wet-chemistry method, which are beneficial for scalable manufacturing for practical applications.

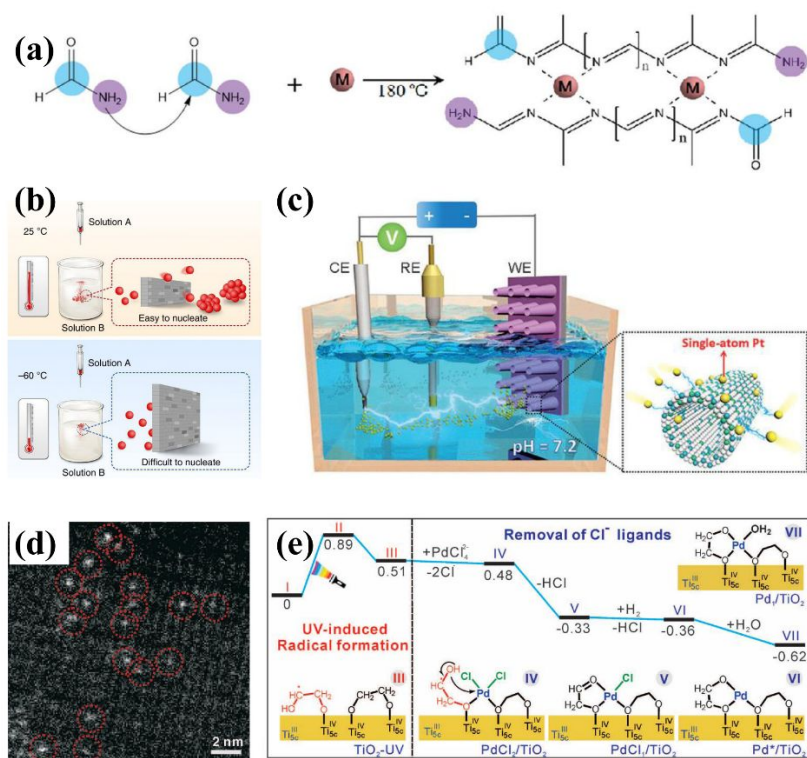


Fig. 1 (a) Chemical crosslinking of FA and metal ions to synthesize SACs. Reprinted with permission from ref. 36. Copyright 2019, The Royal Society of Chemistry. (b) Chemical reduction of ions under $-60\text{ }^{\circ}\text{C}$ to retard the nucleation. Reprinted with permission from ref. 37. Copyright 2019, Nature Publishing Group. (c) Pt dissolution-deposition via electrochemical reduction. Reprinted with permission from ref. 42. Copyright 2017, Wiley-VCH Verlag GmbH & Co. KGaA, Weinheim. (d) Photochemical synthesis of 2D TiO_2 supported Pd SACs, and (e) the mechanism of the radical formation from EG molecules induced by UV and removal of Cl^- . Reprinted with permission from ref. 44. Copyright 2016, American Association for the Advancement of Science.

2.1.1 Chemical reduction. In this approach, a chemical reduction reaction is used to synthesize the 2D materials from chemical compounds, and together with the SAC sites. However, the methods using purely chemical reduction reactions are limited because the nucleation of metals ions under solution can be difficult to control, which often leads to aggregation. There are two ways to tackle this problem. The first one is to use chemical ligands to stabilize the metal ions during the chemical reactions, preventing

their aggregation to form cluster or nanoparticle due to the protective shell effect of the ligands. On the other hand, one can choose the ligand properly, so they can bind with the defect sites, or other nitride sites in the 2D materials, which will facilitate the formation of SACs. Sun's group [35] synthesized single Pt atoms anchored on aniline-stacked graphene by a mild microwave reduction method. Firstly, graphene was functionalized by aniline molecules via π - π interactions with an edge-to-face configuration. Then graphene was positively charged with protonated aniline species ($-\text{NH}_3^+$), which can effectively and uniformly anchor the negatively charged PtCl_6^- to avoid aggregation of metals during the microwave irradiation. However, the efficiency of anchoring metal atoms via this method is low because four anilines can only bind one Pt atom. To improve the low efficiency of anchoring metal atoms, Dai's group [36] reported that formamide (FA) monomer can bond with each other to occur in condensation reaction on the basis of Schiff base reactions and the high N-content ligands in FA (NH_2 group) can chelate with the metals ions to form a cross-linked network. Finally, a high Co loading of 1.5 at% (~ 6.49 wt%) was achieved. They have reported to generate seven types of single-atoms (Fe, Co, Ni, Mn, Zn, Mo, and Ir), bi-metallic (Fe/Co), and tri-metallic (ZnFeCo) electrocatalysts (**Fig. 1a**). Uncontrollable and rapid nucleation/growth hinder the formation of ultrafine nanocrystals or even single atoms in the solution reactions [37]. Besides using the assistant (isolation, anchoring, and stabilization) of chemical ligands, the second approach is to make the nucleation of nanoparticle sluggish. To grow the nanoparticle, the aggregation of the metal ions has to overcome a critical size [38, 39]. On the other hand, the formation of SAC only needs individual metal ion, which has a lower formation barrier. As a result, besides the using of ligand to control the thermodynamics and create nanoparticle nucleation barrier, one can also use temperature to selectively control the process [40]. In general, lower temperature can prevent the formation of nanoparticle, while still be able to synthesize SACs due to their smaller barrier. Wu et al. [37] reported a chemical reduction of Co^{2+} by hydrazine hydrate reductant in the alcohol/water mixed solvent (9:1 in volume ratio) with low freezing point (-78.5 °C). At the temperature of -60 °C, atomically dispersed Co-complex solution was obtained due to the occurrence of an

extremely suppressive nucleation (**Fig. 1b**). Such a method is capable of synthesizing series of SACs (Co, Ni, Cu, Ru, Rh, Pd, Ag, Os, Ir, Pt, Cu) all reduced by NaBH_4 or $\text{N}_2\text{H}_5\text{OH}$ [41].

2.1.2 Electrochemical deposition. Electrochemical deposition is a new wet-chemistry method to synthesize SACs, which initiates the redox reaction controlled by the electric energy in cathode or anode electrodes. Such approach has, previously, been used widely in electroplating. Compared with chemical reduction, electrochemical deposition has high controllability via tuning the current and voltage, the ionic concentration, pH value, deposition time/cycling number, and substrate electrode. Luo et al. demonstrate a potential-cycling method (**Fig. 1c**) [42]. Pt foil is used as a counter electrode and nickel foam supported CoP nanosheet array is used as a working substrate electrode. Potential cycling was performed with a scanning rate of 150 mV s^{-1} between the voltage range of 1.5 and 0.668 V vs. saturated calomel electrode (SCE) in a 1 Mole phosphate buffered saline (PBS) solution at $25 \text{ }^\circ\text{C}$. In this situation, Pt in the counter electrode loses electrons at oxidation voltage and dissolved into the solution to form Pt ions. After that, Pt ions migrate to the working electrodes under the electric field and deposit on the CoP nanosheet arrays [42]. Based on the same rationale, Zeng's group [43] generalized the electrochemical deposition to a universal route fabricating more than 30 different SACs. Moreover, they used two kinds of deposition modes, namely cathodic deposition and anodic deposition. Intriguingly, the same metal elements fabricated by different modes exhibit different electronic structure, which can be used to tune the catalytical properties accordingly.

2.1.3 Photochemical reduction. The photochemical reduction method employs ultra-violet (UV) lights. The mechanisms of photochemical reductions of metal ions include: radical-induced reduction, excited photoelectron or hole formation from semiconductor, and direct irradiation reduction. In 2016, Zheng's group [44] fabricated atomically dispersed Pd SACs (Pd_1/TiO_2) loaded on two-atom-thick TiO_2 2D nanosheets with Pd loading of 1.5 wt% via a room-temperature photochemical reaction (**Fig. 1d and e**). Firstly, the two-atom-thick TiO_2 nanosheets were prepared by reacting TiCl_4 with ethylene glycolate (EG). Then, they showed that UV light can induce

ethylene glycolate (EG) radicals, and this helps to remove of Cl⁻ ligands which is critical to achieve high stability and activity in C=C bond hydrogenation [44, 45]. Besides EG, PVP is also used as the organic ligands to stabilize the single atomic site nature of the photoreduction product. In this case, it is helpful to use TiO₂ [44], C₃N₄ as the supports because the photoexcited electron derived from such semiconducting supports can help to reduce the metal ions into metal atom on the 2D material [46]. However, in Wang's work [47], UV light can directly reduce the PtCl₆²⁻ ions into Pt SACs without using the semi-conducting supports, nor any protective agents. UV light as a fast and novel preparation approach for SACs is worthy of further exploration and its underlying synthesis mechanism needs to be understood better in the future.

Although the wet-chemistry method is a potential mild route for the mass production of SACs, the anchoring metal efficiency needs to be further improved. Additionally, the removal of residual ligand is also a non-negligible problem to avoid coverage or poison of active sites. Noteworthy, the stability of SACs needs to be checked because the anchoring strength of metal atoms on supports achieved by the wet-chemistry approach is usually weak.

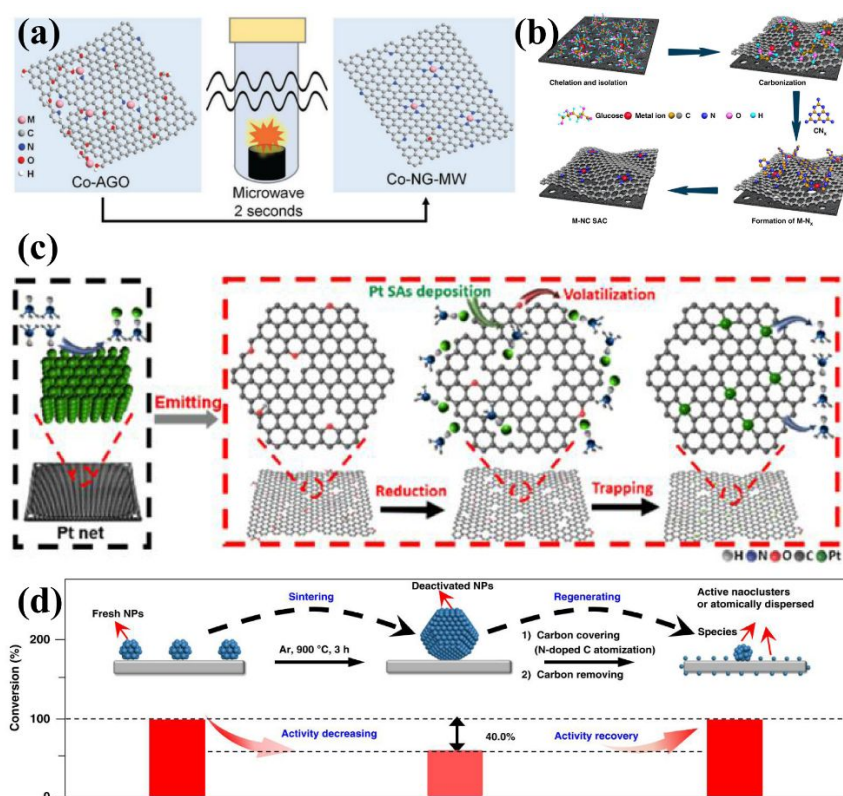


Fig. 2 (a) Rapid microwave-assisted pyrolysis to synthesize SACs in 2 seconds. Reprinted with permission from ref. 59. Copyright 2018, Wiley-VCH Verlag GmbH & Co. KGaA, Weinheim. (b) The cascade anchoring strategy for the synthesis of M-NC SACs with high metal loading. Reprinted with permission from ref. 61. Copyright 2019, Nature Publishing Group. (c) Thermal emitting of Pt SAs from bulk Pt net. Reprinted with permission from ref. 66. Copyright 2019, American Chemical Society. (d) Schematic images of the regeneration of SACs from the sintered NPs by solid diffusion, Pd NPs/TiO₂, Pd NPs/TiO₂-900, and Pd SAs/NPs/TiO₂-900. Reprinted with permission from ref. 74. Copyright 2020, Nature Publishing Group.

2.2 High-temperature pyrolysis strategy

High-temperature pyrolysis of metal precursors is the most common way to prepare SACs to date. Due to the possible high surface entropy, aggregation and coalescence are the key problems in the pyrolysis route. In order to obtain the atomically dispersed sample, pretreatment on the precursor (isolation [48, 49], polymerizations [50-52], coordination [53]), or post-treatment of the pyrolyzed product (acid washing or etching) [54, 55] are usually needed. Notably, one-step pyrolysis can be simple but suffer from low metal loading. Increasing the anchoring force is of great importance, which is usually accomplished by adding N-rich precursors (such as melamine, dopamine [50], dicyandiamide [53, 56]) prior to thermal treatment or calcining the precursors under NH₃ atmosphere [57]. On the other hand, changing the kinetics of precursor decomposition can also prevent aggregation. By strictly controlling the gasification at an ultraslow rate of 1 K/min, Wei and coworkers synthesized Zn SACs with Zn weight content as high as 9.33 wt% [58]. Another extreme approach is to shorten the pyrolysis time as less as possible to prevent the single metal atoms from aggregating. Due to the volume heating mode and extremely rapid heating rate, microwave-assisted pyrolysis is able to synthesize SACs in 1-2 seconds with high dispersity (**Fig. 2a**) [59, 60]. Recently, to accomplish both the general applicability and high loading of SACs, Wan's group developed a cascade anchoring strategy (**Fig. 2b**) [61]. First, metals were chelated by a chelating agent, then anchored on an oxygen-functionalized support (primary

protection). The extra chelating agent can physically isolate the metal complex (secondary protection). Secondly, the mixture was added into melamine, which serves as a nitrogen source for further anchoring in subsequent pyrolysis processes. During pyrolysis, the residue chelating agent can further secure metals ions (tertiary protection), while carbon nitrogen species (CN_{sx}) decomposed from melamine can bind with metal ions to form M–N_x moieties (quaternary protection).

2.3 Solid-diffusion strategy

Similar to the pyrolysis strategy, solid-diffusion methods also need high temperatures as a driven force. However, high-temperature pyrolysis strategy is a bottom-up route, by which ionic precursors are decomposed into atomic species and subsequently anchored by defect, heteroatoms, or ligands. In contrast, the solid-diffusion strategy is a top-down strategy. Bulk materials are used as the precursors, the atomic species escape from the surface of the bulk metals and are captured by the neighboring sample with the assistance of defects or heteroatoms. This method is suitable for volatile metals, such as Pt, Pd, Au, Cu, etc [62-66]. Also, it is more effective to use reducible supports (such as CeO₂, FeO_x, TiO₂, etc.) to form stable SACs due to the strong metal-support interactions [67-69], although MOF-derived or micropores-dominated carbon supports with rich N content can also confine/anchor the single-atom with high stability [64, 70, 71]. In Li's work, Pt net was used to emit the Pt single-atoms, with the assistance of dicyandiamide, forming gaseous Pt (NH₃)_x, which can then be captured by the adjacent graphene support (**Fig. 2c**) [66]. Similarly, it is feasible to use metal salt precursor or oxide (such as FeCl₂ [72] and Fe₂O₃ [73]) as bulk phase together with N doped defective carbon support via “non-contact pyrolysis” to synthesize SACs. The solid-diffusion process can be regarded as the reverse process of aggregation of nanoparticles (NPs), thus it can provide an effective approach to regenerate the SACs or structural repairing of nanocatalysts in practical applications [73-75]. For instance, the deactivated NPs (Pd NPs/TiO₂-900) can be transformed into SACs (Pd SAs/NPs/TiO₂-900) after a N-doped atomization, and the catalytic activity of Pd SAs/NPs/TiO₂-900 in styrene hydrogenation recovers to the original level of fresh catalyst Pd NPs/TiO₂ (**Fig. 2d**) after a solid-diffusion process [74]. To conclude, solid-diffusion strategy as a

reverse engineering of aggregation can provide us with a new approach to synthesize and repair the SACs. However, the random landing of emitted atoms can result in low metal loading since it is difficult to control the deposition sites of the single-atoms.

2.4 Other methods

Whether by using a top-down or bottom-up route, SACs formation needs the reduction, decomposition, or delamination of precursors driven by the input energy. Therefore, various alternative methods, such as ball-milling, ultrasound, and plasma-assisted methods, have been developed. For example, Kim and coworkers have directly constructed Pt SACs via a simple and fast mechanical ball milling method without pyrolysis or reduction process^[76]. A facile dangling bond trapping strategy to construct SACs from bulk metals with the assistance of sonication is developed by Wu et al.^[77]. In this case, the ultrasound plays the role of pulling the surface metal atoms away of the bulk metal, and the escaped atoms are then captured by oxygen functional groups on graphene oxide. More recently, Li and coworkers found that the electrons in plasma can be used as the “green” reductant to directly reduce ions to neutral-atoms, meanwhile, the N fragments in N₂ plasma can be doped into the support to anchor the single-atoms with high stability^[78, 79]. Additionally, chemical-potential-driven replacement reaction is also a facile and attractive approach, which could selectively load metal single atoms on the aimed 2D supports with the help of heteroatoms or vacancy in the hetero-interface, such as the reported Pd/MoS₂^[80] and Pt/NiS₂^[81] SACs.

Although, more and more synthesis techniques have been employed to prepare SACs, the cost of synthesis (including metal reserves and energy consumption), the potential and generality of their scale-preparation, and the stabilities of SACs are important questions to be considered. There are still much room for improvement for the above mentioned preparation strategies for SACs, as shown in **Fig. 3**. Specifically speaking, wet-chemistry method is a potential mild route for the mass production of SACs, but its synthesis generality, single-atom loading, and anchoring robustness need to be further improved. High-temperature pyrolysis is the most commonly used route to synthesis SACs due to its high universality for a wide range of metals, however, the energy consumption and sophisticated device limitation have hindered its scale-up

preparation. Solid-diffusion strategy has its unusual SACs formation mechanism, while, it suffers from finite supports/metals and high energy consumption. Therefore, the innovation of SACs synthesis methodology is still needed and one needs to comprehensively consider its cost-effectiveness, generality, and feasibility of scale-up preparation.

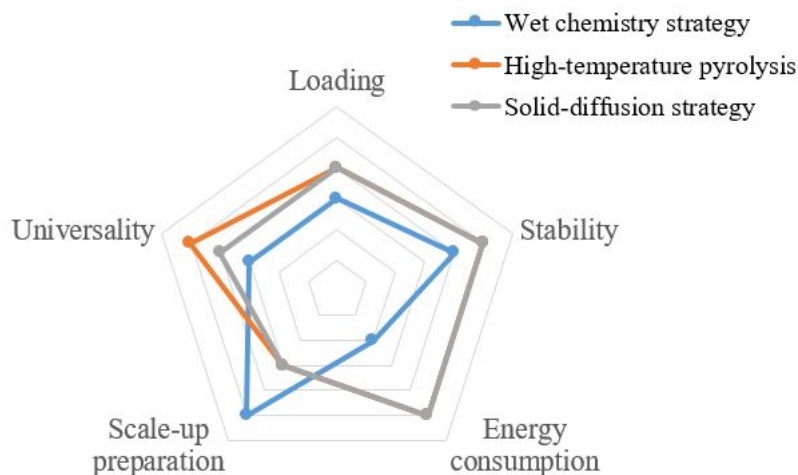


Fig. 3 Comparison of wet chemistry strategy, high-temperature pyrolysis, and solid-diffusion strategy of SACs.

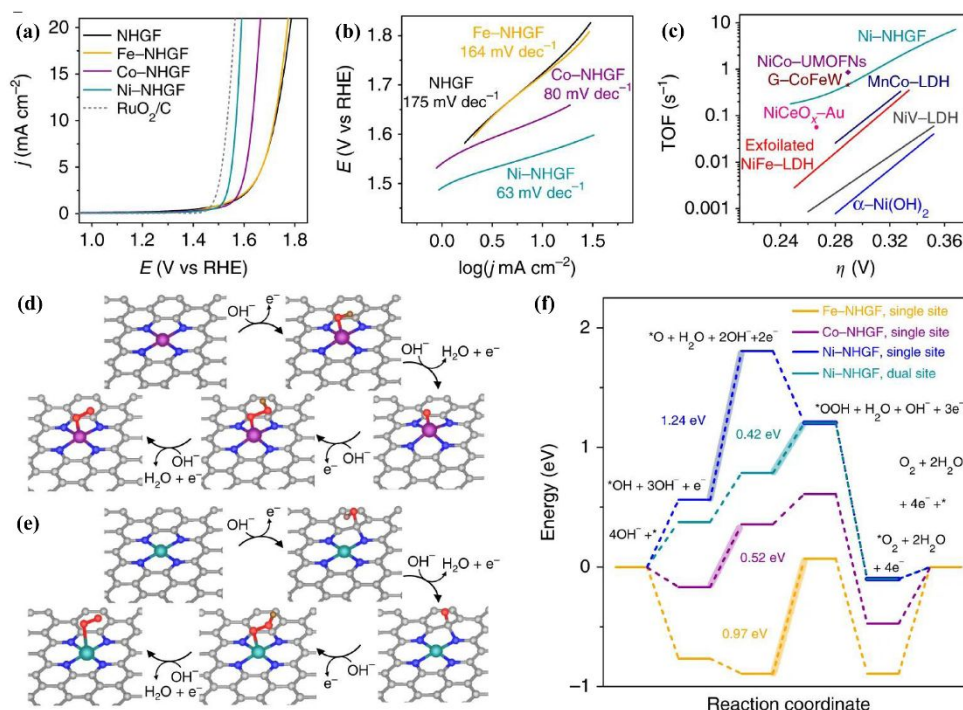


Fig. 4 Catalytic OER performance evaluation of MN_4C_4 electrocatalysts by (a-c) electrochemical measurements and (d-f) DFT calculations. Reprinted with permission from ref. 57. Copyright 2018, Nature Publishing Group.

3. Applications of single-atom catalysts supported on 2D materials for electrochemical OER

The exploitation of high-efficient catalyst is the key to accomplish the low overpotential and high activity toward the four-electron process of OER. In this section, the typical 2D materials (graphene, graphdiyne, LDHs, graphitic carbon nitride, and other 2D materials) supported SACs for OER will be summarized. Their experimental and theoretical representative electrocatalysts including single atom component, valence state, and corresponding OER performance are summarized in **Table 1** and **Table 2**, respectively.

Table 1. OER activity of experimentally reported 2D-SAC electrocatalysts.

2D supports	Catalysts	Single atom	Valence state	Overpotential [mV] @10 mA cm ⁻²	Tafel slope [mV dec ⁻¹]	TOF [s ⁻¹]	Rate determining step	Active site	Electrolyte	Ref.
graphene	Ni-NHGF	Ni	(+2)	331	63	0.72 (300 mV)	O* → OOH*	C, Ni	1 M KOH	[57]
graphene	A-Ni@DG	Ni	-	270	47	13.4 (300 mV)	-	Ni	1 M KOH	[83]
graphene	Ni-O-Gr	Ni	> (+2)	224	42	1.44 (300 mV)	OH* → O*	Ni	1 M KOH	[84]
graphene	Ni ₄ Fe ₁ -O-Gr	Ni, Fe	(+2), (+3)	247	-	1.35 (300 mV)	-	-	1 M KOH	[88]
graphene	SCoNC	Co	0-(+2)	310	74	-	O* → OOH*	Co	0.1 M KOH	[49]
graphdiyne	Ru/GDY	Ru	-	531	100	7.09 (770 mV)	-	Ru	0.5 M H ₂ SO ₄	[90]
NiFe LDH	^s Au/NiFe LDH	Au	-	237	36	0.11 (280 mV)	O* → OOH*	Fe	1 M KOH	[104]
CoCr LDH	CoCrRu LDHs	Ru	-	290	56	-	OH* → O*	Co	0.1 M KOH	[107]
CoFe LDH	Ru/CoFe-LDHs	Ru	(+1.6)	198	39	-	O* → OOH*	Fe, Ru	1 M KOH	[105]
Co(OH) ₂	CoIr-0.2	Ir	0, (+4)	373	117.5	-	-	Ir	1 M PBS	[108]
			0, (+4)	235	70.2	-	-	Ir	1 M KOH	
α-Ni(OH) ₂	w-Ni(OH) ₂	W	(+6)	237	33	0.74	OOH* → O ₂	W	1 M KOH	[109]

g-C ₃ N ₄	Co-C ₃ N ₄	Co	(+2)	380	68.4	-	O* → OOH*	Co	1 M KOH	[110]
g-C ₃ N ₄	Au ₁ N _x /g-C ₃ N ₄	Au	-	450	112	-	-	Au	0.1 M KOH	[111]
g-C ₃ N ₄	Ru-N-C	Ru	(+3)-(+4)	267	52.6	3.72 (300 mV)	O* → OOH*	Ru	0.5 M H ₂ SO ₄	[112]
g-C ₃ N ₄	NiFe@g-C ₃ N ₄ /CNT	Ni, Fe	-	326	67	-	-	-	1 M KOH	[113]

Table 2. OER activity of theoretically reported 2D-SAC electrocatalysts.

2D supports	Catalysts	Overpotential [V]	Rate determining step	Medium	Ref.
graphene	4N-Co	0.39	O* → OOH*	Acidic	[86]
graphdiyne	Ni@GDY	0.29	O* → OOH*	Acidic	[91]
graphyne	Co@GY	0.55	O* → OOH*	Acidic	[92]
graphyne	Co@N ₁ -GY	0.42	O* → OOH*	Acidic	[93]
graphyne	Co@GY/Ni@GY	0.38	OH* → O*	Acidic	[95]
g-CN	Co@g-CN	0.16	O* → OOH*	Alkali	[114]
g-CN	Co-O@g-CN	0.41	O* → OOH*	Alkali	[114]
C ₂ N	Mn ₁ @C ₂ N	0.67	OOH* → O ₂	Acidic	[115]
C ₃ N	Rh-V _{CC}	0.35	O* → OOH*	Acidic	[116]
C ₉ N ₄	Ni@C ₉ N ₄	0.31	OH* → O*	Acidic	[117]
Pc	Ir@Pc	0.41	O* → OOH*	Acidic	[118]
COF	Fe-COF	0.38	O* → OOH*	Acidic	[119]
Boronene	Ni1/β ₁₂ -BM	0.40	OH* → O*	Acidic	[124]
Boronphane	Rh-BH	0.24	OH* → O*	Acidic	[125]
BC ₃	Co@V _B	0.43	O* → OOH*	Acidic	[126]
MXene	Nb ₂ CF ₂ -V _F -Pt	0.37	O* → OOH*	Acidic	[128]
MXene	Ni/Cr ₂ CO ₂	0.46	O* → OOH*	Acidic	[129]
MXene	Cu-Ti ₂ NO ₂	0.24	OOH* → O ₂	Acidic	[130]
MXene	Pd ₁ @ Ti ₃ C ₂ O ₂	0.31	OH* → O*	Acidic	[131]

3.1 SACs on 2D carbon-based supports for OER

Carbon-based materials are widely used as the supports due to their high surface area, good chemical stability and good electric conductivity [82]. The original carbon materials like graphene are usually inert to OER before they are modified. Introducing the single atom metal sites and tuning the coordination numbers of these single atom sites are two common ways to improve their OER performance. To prevent the

aggregation of metal atoms on 2D carbon-based supports, their large pore structures, defects, or heteroatom-dopants are used to tightly anchor single metal atoms. Meanwhile, different kinds of bonds are formed between metal atoms and supports, such as C-M^[83], C-N-M^[57] and C-O-M^[84] bonds (M refers to the metal atom).

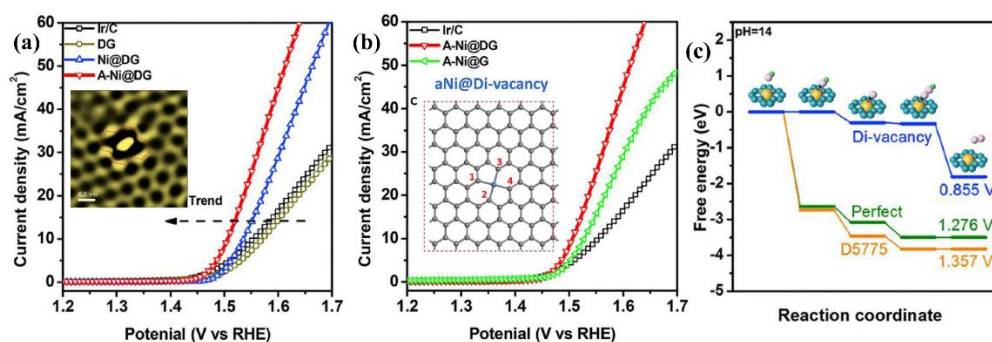


Fig. 5 OER polarization curves of (a) A-Ni@DG, Ni@DG, DG and Ir/C performed in 1 M KOH electrolyte, (b) role of carbon defects of catalysts, (c) Energy profiles of carbon defects for OER. Reprinted with permission from ref. 83. Copyright 2018, Elsevier Inc.

3.1.1 Graphene-based SACs for OER. Graphene or graphene-like material is an excellent 2D carrier to load SACs due to its high conductivity and large in-plane surface. Metal species and the surrounding heteroatom-dopant (such as B, N, S, etc.) on graphene are the two major factors that determine the OER activity. The challenge is that only a few studies have precisely controlled the configuration of the SACs. In one example, Huang et al. synthesized a series of transition metal SACs (Fe, Co, Ni) embedded in the nitrogen-doped graphene. The influence of the metal species was systematically investigated (**Fig. 4**)^[57]. The extended X-ray absorption fine structure (EXAFS) spectrum combined with an annular dark-field scanning transmission electron microscope (ADF-STEM) unambiguously revealed that the structure of catalyst is MN₄C₄ motif rather than MN₄C₈ and MN₄C₁₂. The activity shows a descending trend Ni > Co > Fe for OER both by experimental measurement and theoretical calculations. The OER overpotential for Ni-NHGF was 331 mV at a current density of 10 mA cm⁻², while the values for Fe-NHGF and Co-NHGF were measured to be 488 and 402 mV at 10 mA cm⁻², respectively. Besides, the Tafel slopes follow the same trend: Fe-NHGF (164 mV dec⁻¹) > Co-NHGF (80 mV dec⁻¹) > Ni-NHGF (63 mV dec⁻¹).

The turnover frequency (TOF) results for these SACs also indicated that the Ni-NHGF is the best OER electrocatalyst in this series. According to the DFT calculations (**Fig. 4d-f**), it is found that the OER performance was intimately related to the number of d orbital electrons (N_d) of the M in the MN_4C_4 motif. Specifically, for Fe ($N_d = 6$) and Co ($N_d = 7$) SACs, all oxygenated intermediates (OH^* , O^* , OOH^*) preferred to be absorbed on M site rather than on C site. For Ni ($N_d = 8$) SAC, O^* and OH^* prefer to bind with the C site, while the OOH^* favors to bind with the Ni site. Therefore, FeN_4C_4 and CoN_4C_4 SACs experience the single-site mechanism while NiN_4C_4 favors the dual-site mechanism. The free energy diagram shows that NiN_4C_4 in Ni-NHGF sample via dual-site mechanism exhibits an energy barrier of 0.42 eV in the rate-determining step (RDS) from O^* to OOH^* , which is significantly lower than that of FeN_4C_4 (0.97 eV) and CoN_4C_4 (0.52 eV). Compared with the single-site mechanism of SACs, this dual-site mechanism of Ni-NHGF not only helps to decrease the energy barrier but also illustrates the mutual benefits between metal active center and the 2D support. Besides the most common N-coordinated Ni SACs, other configurations of Ni single atom, such as defect anchored, O atom coordinated, and N, S co-modified Ni SACs have also been reported to have highly activity to OER. A Ni single atoms embedded in defective graphene (A-Ni@DG) for OER in alkaline media were reported in Yao's work [83]. The di-vacancy anchored Ni SACs over graphene was directly observed by HADDF-STEM technology as having a four-coordinated NiC_4 structure (**Fig. 5**). This as-synthesized A-Ni@DG SAC exhibited improved OER performance with an overpotential of 270 mV at the current density of 10 mA cm^{-2} (**Fig. 5a and b**). Moreover, the A-Ni@DG electrocatalyst also shows perfect stability during long-lasting tests, which can be attributed to the strong binding between the Ni atom and the di-vacancy on the graphene support. Besides, DFT calculations suggest that the defect structure in graphene can significantly influence the electronic structure of Ni single atoms, and Ni embedded in the di-vacancy defect of graphene has the optimal electronic structure for OER (**Fig. 5c**). Li and coworkers are the first to synthesize oxygen-bonded Ni-O-Gr SACs on graphene-like carbon [84]. In this case, the higher electronegativity of O (3.5) (compared to the 1.8 value of Ni) leads to a highly positively charged Ni atoms with a high theoretical

oxidation state (+2.34). Consequently, the catalyst with high-valence Ni exhibited an extremely low overpotential of 224 mV at 10 mA cm⁻², a small Tafel slope of 42 mV dec⁻¹, and oxygen production TOFs of 1.44 and 2.81 S⁻¹ at the overpotential of 300 and 350 mV, respectively (**Fig. 6a and b**). Moreover, at a high current of 115 mA cm⁻², Ni-O-Gr SAC exhibited long term stability without obvious decay over 50 h (**Fig. 6c**), surpassing its counterpart of N-bonded SACs (Ni-N-G SACs) and Ni(OH)₂ nanoparticles anchored on graphene (Ni(OH)₂/G). Furthermore, DFT results reveal that in the Ni-O₄(OH)₂ structure, the bonding between single Ni atoms and the O sites, which formed high oxidation state of the Ni species, lead to low OER overpotential and significantly reduced Gibbs free energy barrier for Ni-O-Gr SACs (**Fig. 6d and e**). Xu et al. also reported a similar strategy for fabricating single Ni atom bonded with O on reduced graphene. The synthesized Ni SACs display good OER electrocatalytic activity [85].

Besides graphene supported Ni SACs, other metal (like Fe and Co) with specific features (optimized coordination, bi-metal synergy, high metal loading) can also deliver a superior OER performances. For example, Zhou et. al theoretically demonstrates that the higher coordination number Co site on nitrogen decorated graphene (4N-Co) is a promising OER electrocatalyst with a low calculated overpotential of 0.39 V. Additionally, the presence of p states of the N atom and d states of Co around the Fermi energy suggest the strong hybridization between the N and Co atom, indicating the strong binding between N and Co atom [86]. N and S co-decorated and atomically dispersed Fe-N_x species show better performance than individually doped Fe [87]. The synergy between Ni and Fe single atoms with an optimized ratio of 4:1 can deliver a better OER performance (a small overpotential of 247mV at 10 mA·cm⁻²) than the corresponding single specie counterparts (329 mV for Ni SACs and 384 mV for Fe SACs) [88]. Huang and co-workers reported a densely populated Co-SAC on graphene-like N-carbon support (SCoNC) [49]. The fraction of single Co on the possible binding sites in SCoNC reaches ≈15.3%. This leads to a high electrochemically active surface area of ≈105.6 m² g⁻¹. The SCoNC catalyst achieves a current density of 10.0 mA cm⁻² at 1.54 V with a Tafel slope of 74 mV dec⁻¹ for OER measurement.

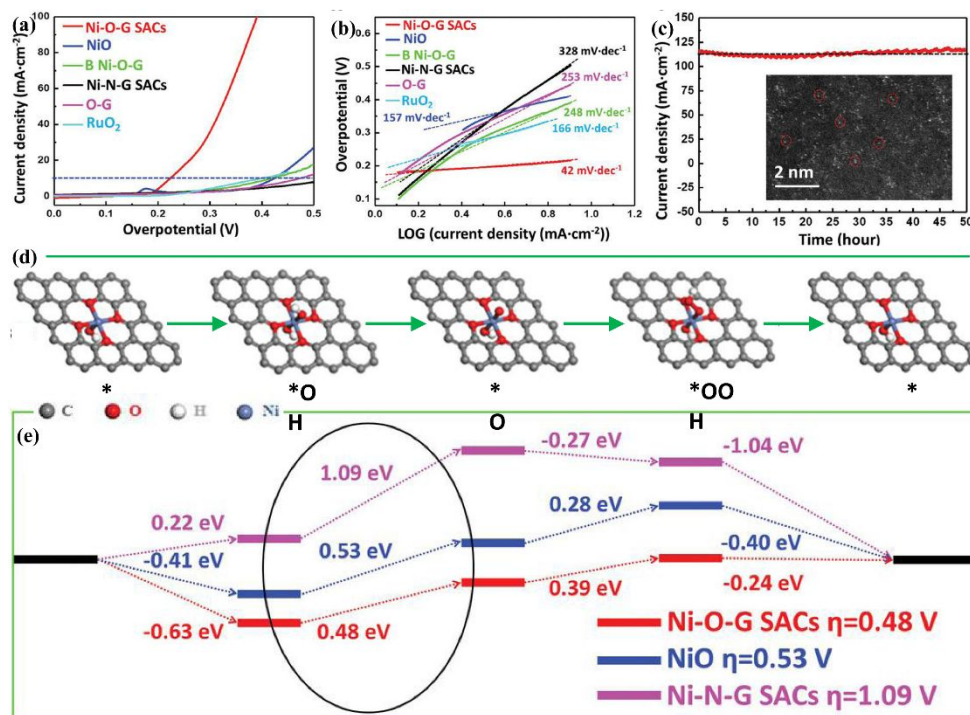


Fig. 6 Catalytic OER performance evaluation of Ni-O-G SACs electrocatalysts by (a) Polarization curves, (b) Tafel slope, (c) Stability, and (d-e) DFT calculations. Reprinted with permission from ref. 84. Copyright 2020, Wiley-VCH Verlag GmbH & Co. KGaA, Weinheim.

3.1.2 Graphdiyne-based SACs for OER. Graphdiyne (GDY) containing sp - and sp^2 -hybridized carbon atoms is the first experimentally synthesized member in the graphyne family^[89]. GDY can be used as the substrate material in the synthesis of SACs due to its excellent chemical stability, rich carbon chemical bonds environments, high π -conjunction, wide surface spacing, and tunable electronic properties. Li and co-workers designed a zero-valence Ru atomic electrocatalyst on GDY (Ru/GDY) with the help of DFT calculations^[90]. The as-synthesized Ru/GDY electrocatalyst exhibited high catalytic activity for OER in the 0.5 M H_2SO_4 solution with an OER overpotential of 531 mV at 10 mA cm^{-2} . When compared with the Ru NP/GDY, pristine GDY, and carbon cloth, the Ru/GDY SAC possess the smallest Tafel slope of 100 mV dec^{-1} , the largest j_0 of 0.084 mA cm^{-2} (a large j_0 means that a high current density can be obtained at a small applied voltage), and the highest TOF (7.09 s^{-1} at 2.0 V vs RHE) (**Fig. 7a and b**). The 2000 OER cycling test for 54 h demonstrates the robust stability of the Ru/GDY SAC in

acidic media (**Fig. 7c**). After the stability test, they found that there was almost no changes in the morphology and chemical states of catalysts. The DFT calculations illustrates that the strong Ru-C coupling in the Ru/GDY electrocatalyst makes the zero-valent Ru atoms to be the unique electron-mediating-vehicle for fast reversible redox-switching, leading to high OER catalytic activity (**Fig. 7d-f**). In a follow up work, based on DFT calculations, He and co-workers studied 11 transition metal species supported on GDY (TM@GDY) as OER electrocatalysts and screened out the best electrocatalyst: Ni@GDY, which has an OER overpotential of only 0.29 V ^[91]. Gao and co-workers explored a series of graphyne (GY) anchored transition metal (from Sc to Zn) SACs for water-splitting via theoretical calculations ^[92]. The Co@GY catalyst stands out from the 10 designed SACs due to its relatively low theoretical OER overpotential (0.55 V). Then, the OER overpotential of Co@GY was further improved to 0.42 V by doping N atom into the Co@GY catalyst. The improvement of the resulting (Co@N₁-GY) is attributed to the increased charge density on Co, which repels the adsorption of OH*, O*, and OOH* intermediates with different degrees ^[93]. Moreover, when applied a biaxial tensile strain of 3% on the Co@N₁-GY SAC, it exhibits a minimum OER overpotential of 0.33 V ^[94]. On the other hand, the OER performance of the 2D Co@GY catalyst is also dramatically influenced by its adjacent TM@GY (TM = Mn, Fe, Co, Ni, Cu) layers ^[95]. A volcano-type trend of OER catalytic performance as a function of $\Delta G^*_{\text{OOH}} - \Delta G^*_{\text{O}}$ was obtained, showing that the Co@GY/Ni@GY catalyst has a lowest OER overpotential of 0.38 V.

3.2 SACs on 2D LDH supports for OER

Layered double hydroxides are a kind of 2D materials that composed of positively charged edge-sharing MO₆ octahedral layers and charge-compensation anions, which can be expressed by the general formula as M^{II}_{1-x}M^{III}_x(OH)₂(Aⁿ⁻)_{x/n}·yH₂O, where M^{II} and M^{III} are metallic divalent cations and trivalent cations, and Aⁿ⁻ is the intercalated anion ^[96, 97]. Numerous literature has shown that LDH themselves are promising OER catalyst because of its tunable chemical composition, including single component LDH, such as Ni(OH)₂, Co(OH)₂, and binary LDH, like NiFe- ^[98], NiCo- ^[99, 100], CoFe- ^[101-103], CoMn-LDH ^[97]. OER normally occurs on the edge sites rather than on the in-plane

surface of LDH. Therefore, further modification, like doping, surface sulfidation, and defect engineering [101, 102], are employed to maximize the utilization of the active sites. Recently, several works which combine single atom site component with the LDH support have emerged. Single metal atoms are generally anchored on the top surface of LDHs and bonded with the O atoms that in MO_6 units to form M_1-O-M_2 bonds (M_1 refers to the single metal atom, M_2 refers to the metal site in LDH) [104, 105]. The synergetic effects between LDH and the single-atom sites enhance the OER activity. More specifically, the synergetic effect can origin from (1) optimization of the electronic structure at active sites on LDH [104]; (2) increased in-plane active sites contributed from single atoms on the LDH support [105]; (3) surface reconstruction of the surface sites under the dynamic evolution process [106].

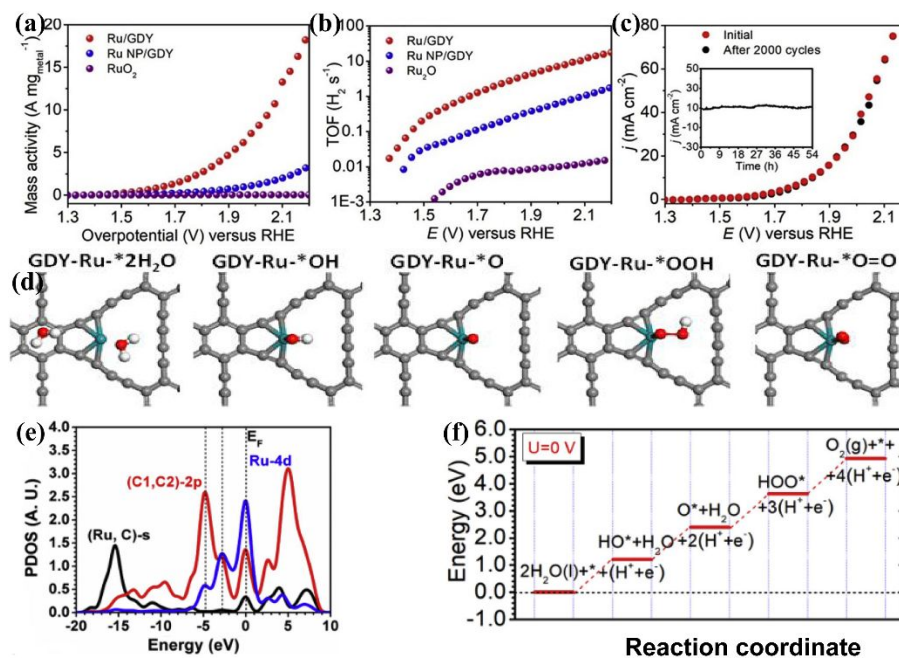


Fig. 7 OER performance of Ru/GDY electrocatalyst: (a) mass activity, (b) TOF value, (c) Polarization curves before and after 2000 OER cycle; OER mechanism from DFT calculations: (e) PDOS, (f) OER energetic pathway. Reprinted with permission from ref. 90. Copyright 2020, Elsevier Ltd.

In 2018, using electrodeposition method, Zhang and coworkers synthesized NiFe LDH supported Au SAC ($^sAu/NiFe$ LDH) to evaluate their OER activity and reaction mechanism (**Fig. 8**) [104]. Notably, the theoretical calculation results reveal that the

active sites are not Au atoms but Fe atoms in ^sAu/NiFe LDH. The decoration of 0.4 wt% Au atoms onto the NiFe LDH exhibits a 6-fold enhancement on the OER activity with respect to the pure NiFe-LDH. Au atoms play a role in changing the charge distribution of active Fe and its surrounding atoms. The 5d orbitals of Au are spatially redistributed after the adsorption of Au on O that give rise to the charge density around Au. A net charge of 0.32 *e* is transferred from the Au atom to the surrounding O, Ni and Fe atoms, which facilitates the adsorption of OH⁻ and moderates the binding strength of O* and OOH* on the catalyst. The calculated results show that the rate-limiting step is the formation of OOH* from O* in the presence of Au, which exhibits a lower overpotential (0.18 V) than that of the counterpart without Au (0.26 V), where the rate-limiting step is the formation of O* from OH*. The experimental results showed that the OER overpotential for the NiFe LDH and ^sAu/NiFe LDH catalysts were 263 and 237 mV at 10 mA cm⁻², respectively, roughly agreeing with the theoretical results. The in-situ transformation of LDH to NiFe oxyhydroxide under the OER potential agrees with the theoretical results that the in-situ generated oxyhydroxide serves as the OER catalytic centers. A similar conclusion was also reported by Huang's work, which uses a Ru doped CoCr LDHs (CoCrRu LDHs) as a model electrocatalyst for OER [107]. The synthesized CoCrRu LDHs with lattice point defects exhibit improved OER performance. In 0.1 M KOH, CoCrRu LDHs reaches 10 mA cm⁻² current density with only 290 mV OER overpotential and it has a Tafel slope of 56.12 mV dec⁻¹ (**Fig. 9a and b**). Furthermore, DFT calculations illustrated that the atomic Ru dopant acts as an electron reservoir, which activates the adjacent Co atoms in CoCrRu LDH to optimize the adsorption of the reaction intermediates. More specifically, Ru dopants downshift d states of Co and enhance the electron donation of Cr to oxygenates, which ultimately weakens the adsorption of OH* and O* on the Co atoms, and strengthens the adsorption of OOH* (**Fig. 9c and d**). This behavior breaks the theoretical scaling relationship, which relates the adsorption strengths among HO*, O* and OOH* and limits the optimization of OER overpotential. The above works show that the atomic site is just a "promoter" of the real active sites on LDHs, instead of the actual binding site. It can change the electronic structure of the active site in the original LDHs. Recently, Li and

coworkers have synthesized a stable single atomic ruthenium catalyst anchoring on the surface of cobalt iron layered double hydroxides (Ru/CoFe-LDHs) by forming Ru-O-M bond (M refers to Fe or Co) [105]. The Ru/CoFe-LDHs electrocatalyst with 0.45 wt% Ru loading shows an excellent OER performance, requiring only 198 mV overpotential to reach 10 mA cm^{-2} in alkaline solution. It also has a small Tafel slope of 39 mV dec^{-1} (**Fig. 10a and b**). DFT+U simulation proved that both the Fe atoms at the edge of CoFe-LDHs and the Ru atoms on the plane surface that coordinated with five oxygen atoms on Ru/CoFe-LDHs are the active sites for OER (**Fig. 10c and d**). The Gibbs free energy of the rate-determining step for the Ru atom sites on Ru/CoFe-LDHs was 1.52 eV, which is lower than that of the Fe atom sites at the edge of CoFe-LDHs (1.94 eV) (**Fig. 10e and f**). Additionally, from the XPS and differential charge density analysis, they found that the electrons transfer from Co or Fe to Ru, indicating the strong electron coupling between monoatomic Ru with CoFe-LDH support. Therefore, the introduction of Ru can increase the extra active sites from the on-plane surface and boost OER activity with strong synergetic electron coupling between Ru and LDHs substance. More importantly, this strong electronic coupling interaction could allow Ru atoms exist at a valence state of 1.6+ while stably work below 4+ without facing the dissolution problem. Considering that the OER is operated under oxidation potential, the impact of the dynamic evolution of the catalysts during OER process and the related stability has attracted a lot of attentions recently. Song and coworkers reported their works of Co(OH)_2 nanosheet supported Ir SAC for the OER [108]. They found an oxidation process evolving from $\alpha\text{-Co(OH)}_2$ with atomic Ir species to the more stable $\beta\text{-CoOOH}$ with high valence Ir species. They believe the reconstruction-derived high valence Ir species with a low-coordination structure is responsible for the superior OER performance. This work demonstrates a phase transformation process of the LDH which can synergistically promote the OER activity. However, the active site was not identified in their work. More recently, the dynamic stability of the active site over LDH under oxidative environment was reported by Chung et al [106]. In the model $\text{Fe-MO}_x\text{H}_y$ ($M = \text{Mn, Fe, Co, Ni, Cu}$), it is shown that a balance between the rates of Fe dissolution and redeposition over a MO_xH_y host can establish a dynamically stable Fe active site. They proposed that Fe-M adsorption

energy can serve as a general descriptor for the dynamical stability. By enhancing the Fe-M adsorption energy, the interaction between Fe and MO_xH_y would be stronger, whilst yielding more active sites with dynamic stability. Rather than the static active sites, the authors proposed the dynamically stable Fe atoms are the true active sites during the continuous dissolution and redeposition processes of OER. Predicted by the DFT calculation, activity enhancement is clearly predicted on the right side of Fe in the periodic table. This enhancement is the highest for CuO_xH_y , consistent with the experimental observations.

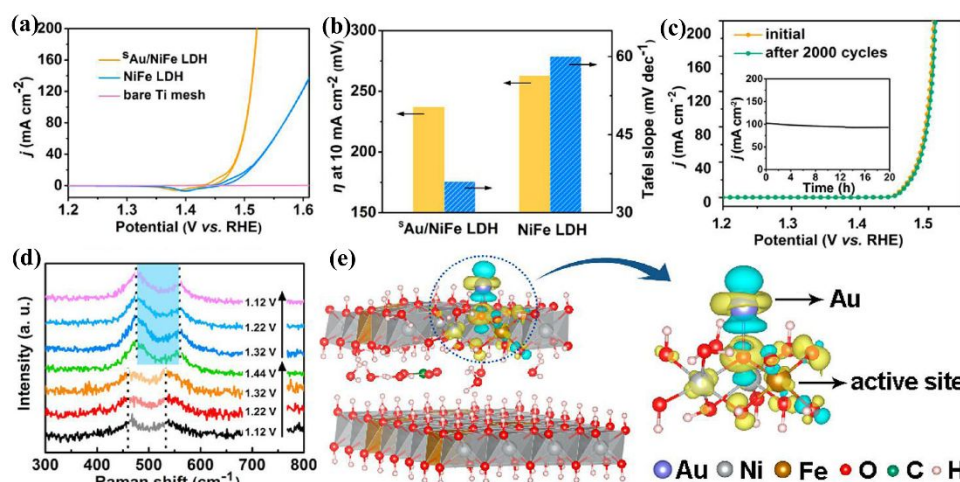


Fig. 8 OER activity of $^s\text{Au}/\text{NiFeLDH}$: (a) CV curves in 1 M KOH, (b) Overpotential at 10 mA cm^{-2} and Tafel slope, (c) Polarization curves before and after 2000 cycles. (d) Raman spectra of $^s\text{Au}/\text{NiFe LDH}$ at different potentials in a cyclic voltammetry cycle. (e) Differential charge densities of NiFe LDH with and without Au atom when one O atom is adsorbed on the Fe site. Reprinted with permission from ref. 104. Copyright 2018, American Chemical Society.

Although the above works have claimed that the synergistic effects between a single atom and LDHs can boost the OER performance, it is still a topic for further investigations, especially for the structure-activity relationship for LDH supported SACs. Whether a single atom itself can form an active site or just act as an electron modulator needs to be further investigated. For example, just changing the LDH type from CoFe LDH to CoCr LDH, the role of Ru atom changes accordingly [105, 107]. The dynamic evolution of LDH supported SACs is an intriguing idea. Some operando

techniques are needed to confirm this claim and to reveal how LDHs cooperate with SACs to enhance the OER activity and stability. Additionally, most of the works focus on the precious single atoms species: Au [104], Ir [43, 108], and Ru [105, 107] on 2D LDHs. Few works regarding the non-noble metal single atoms (e.g., W [109]) were reported. The future development of cost-effective LDH supported SACs should be emphasized.

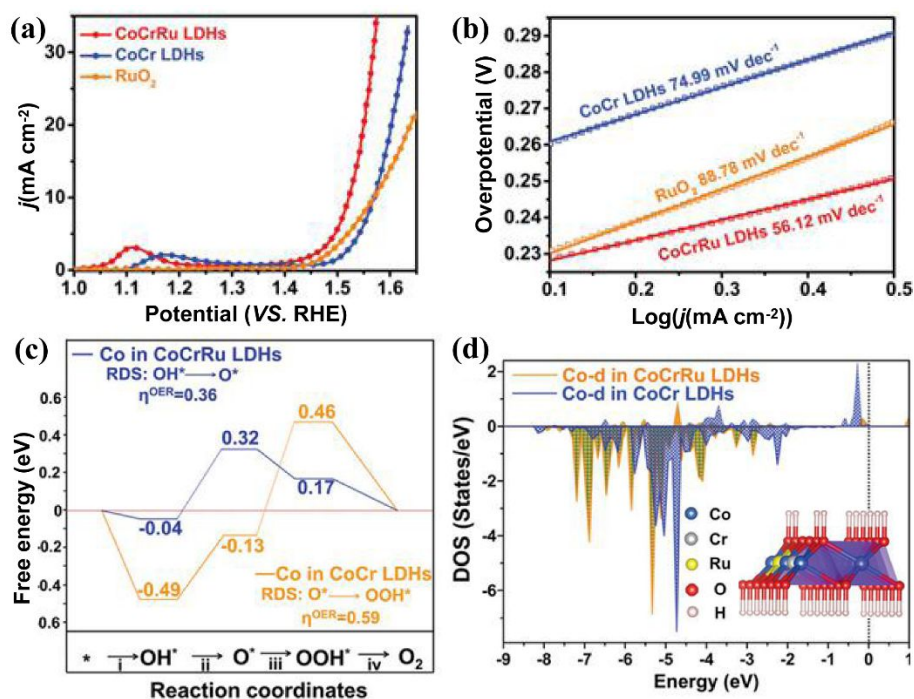


Fig. 9 Linear sweep voltammetry curves (a) and Tafel slope plots (b) of CoCrRu LDHs, CoCr LDHs, and RuO₂ electrocatalysts. (c) Free energy diagrams of OER on the Co sites at equilibrium potential. (d) The projected density of states of Co atoms, and the inset is schematic two-layer slab model for CoCrRu LDHs. The dashed line in (c) and (d) is the rate determining step of OER and the Fermi level, respectively. Reprinted with permission from ref. 107. Copyright 2020, Wiley-VCH Verlag GmbH & Co. KGaA, Weinheim.

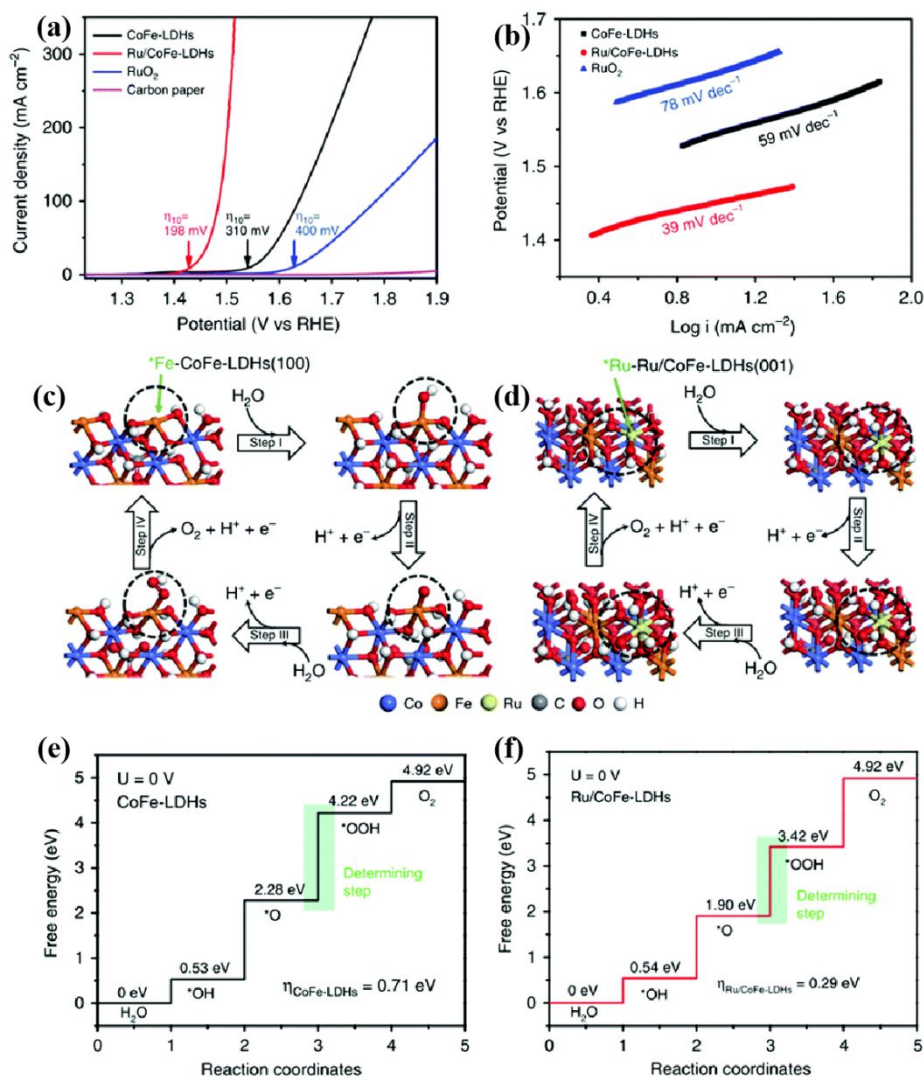


Fig. 10 (a) Polarization curves and (b) the corresponding Tafel plots of Ru/CoFe-LDHs, CoFe-LDHs, and the commercial RuO₂ catalyst. Proposed 4e⁻ mechanism of OER and corresponding Gibbs free-energy diagram on CoFe-LDHs (c and e) and Ru/CoFe-LDHs (d and f) with DFT+*U* calculation, respectively. Reprinted with permission from ref. 105. Copyright 2019, Nature Publishing Group.

3.3 SACs on 2D carbon nitride supports for OER

2D carbon nitride allotropes have a chemical formula C_nN_m, where n and m refer to the number of C and N atoms in the primitive lattice, respectively. Due to the formation of C-C and C-N covalent bonds in the 2D carbon nitride materials, these allotropes are usually rather stable. With different compositions and structures of the C and N atoms, C_nN_m can exhibit different physical and chemical properties. These allotropes offer surface engineering possibilities and have found many promising applications in

catalysts.

3.3.1 SACs on 2D graphitic C₃N₄ (g-C₃N₄) supports for OER. The inert g-C₃N₄ with simplex pyridinic-type nitrogen in the periodic heptazine units can provide multiple electron lone pairs to anchor metal species. The inert g-C₃N₄ can be electrochemically activated by doping with metal species. Besides, the single metal atom doped C₃N₄ can give the unambiguous information about the active site due to the relatively simple structure of C₃N₄. In 2017, Qiao et al. designed a g-C₃N₄ coordinated transition metal SACs M-C₃N₄, including the metal species M = Cr, Mn, Fe, Co, Ni, Cu, and Zn as proof-of-concept electrocatalysts for OER in alkaline condition. Co-C₃N₄ was screened out as having the optimal OER performance^[110]. Experimental and theoretical results proved that the precise M-N₂ coordination in the g-C₃N₄ matrix was the original of the high activity of the OER. Liu and coworkers confined single Au atoms in g-C₃N₄ to form organometallic Au₁N_x moieties as bifunctional efficient and durable electrocatalyst for OER and ORR^[111]. The individually dispersed Au¹⁺ cation can be grafted onto g-C₃N₄ via the formation of the Au-N bond. The Au₁N_x moieties were confirmed as the active site for OER via the combination of experimental and theoretical studies. Later, carbon nitride supported Ru SACs with Ru₁-N₄ motif was reported by Cao et al^[112]. However, through the *Operando* synchrotron radiation X-ray absorption spectroscopy and infrared spectroscopy, the author found the dynamic oxygen adsorption behavior on the Ru₁-N₄ site under the working condition (constant potential of 1.5 V versus RHE in O₂-saturated H₂SO₄ electrolyte). More specifically, the first step is the transformation/activation of the Ru₁-N₄ site to the O-Ru₁-N₄ site, which downshifts the Ru 4d band, resulting in greater covalency of the Ru-N/O bond. Meanwhile, the Ru atom donates its electrons mainly to the adjacent N atoms and it adsorbs the O atom through orbital hybridization in O-Ru-N-C. This optimizes the binding energies with OH*, O* and OOH* intermediates. Consequently, the O-Ru₁-N₄ site under operando condition has a low barrier of O-O formation to form the OOH* intermediate, which enhances the OER activity. They found that the average bond length of Ru-N in catalyst under working condition is 2.05 Å, which is slightly shorter than that of Ru-N (2.08 Å) in the ex situ sample. The slight shrinkage in Ru-N bonds

could further fix Ru atom on the surface, thus avoiding possible dissolution when facilitating OER and improving the stability of the catalyst. Moreover, they found that the morphology and structure remain nearly unchanged after long time electrolysis, as demonstrated by the results of X-ray diffraction (XRD), transmission electron microscope (TEM), and X-ray absorption fine structure (XAFS). Liu et al. reported that by using a Ni and Fe atoms codoping strategy on g-C₃N₄, the Ni and Fe atoms can form a dual-metal (Ni, Fe) active sites on g-C₃N₄ [113]. The Ni, Fe codoped g-C₃N₄ induced a bimetal synergetic effect, endowing NiFe@g-C₃N₄ with a low OER overpotential of ≈ 326 mV at 10 mA cm⁻² and a small Tafel slope of 67 mV dec⁻¹.

3.3.2 SACs on other 2D C_nN_m supports for OER. Besides 2D C₃N₄, other 2D C_nN_m materials have also been used to study their OER activities, such as g-CN, C₂N, C₃N, and so on. Based on DFT calculations, Li and coworkers evaluated the OER activities in the water-alkali media for g-CN monolayer supported transition metal (TM = Pd, Ni, Co, Pt, Cu) TM@CN SACs [114]. The results suggest that TM@CN and TM-O@CN can serve as promising OER electrocatalysts with low-costs, high-durabilities and high-efficiencies. Moreover, the non-noble metal Co-O@CN and Co/Ni@CN SACs exhibit excellent OER activity with low overpotentials. Zhang et al. screened a series of transition metal atoms confined on the C₂N monolayer (TM_x@C₂N) as electrocatalysts for OER [115]. Ab initio molecular dynamic (AIMD) simulations show that the confined TM atoms do not diffuse, suggesting good stabilities of TM_x@C₂N. Among all the TM_x@C₂N SACs, the Mn₁@C₂N was selected as having the lowest OER overpotential of 0.67 V. Zhou et.al have studied a wide range of single transition metal atoms embedded in the double carbon vacancy of C₃N monolayer (TM-V_{CC}) as OER electrocatalysts [116]. Rh-V_{CC} shows the lowest OER overpotential of 0.35 V, followed by Co-V_{CC} (0.43 V). Furthermore, Rh-V_{CC} and Co-V_{CC} possess energy barriers of 1.96 and 2.47 eV to diffuse from the defect adsorbed site to the neighboring hollow site, suggesting the stability of the single catalytic sites. AIMD simulations results also confirmed the good stabilities of Rh-V_{CC} and Co-V_{CC}. Recently, Zhou et.al have designed ten different single transition metal atoms doped on C₉N₄ monolayer (TM@C₉N₄) as OER electrocatalysts [117]. The strong hybridization between the p orbitals of N and the d orbitals of TM atoms suggest the chemical bonding

of N and TM atoms, indicating strong interactions between TM atoms and C_9N_4 monolayer. The theoretical results indicate that $TM@C_9N_4$ SACs are metallic with good electric conductivities. $Ni@C_9N_4$ was screened out as a promising OER electrocatalyst with a low overpotential of 0.31 V. Ir atomically doped phthalocyanine ($Ir@Pc$) is theoretically proved to be an efficient OER electrocatalyst with overpotential of 0.41 V [118]. The negative binding energy, high diffusion energy barrier and positive dissolution energy properties of $Ir@Pc$ indicate its high dispersibility and stability.

3.4 SACs on other 2D material supports for OER

Covalent organic frameworks (COF), as an emerging framework materials linked by covalent bonds, have shown promise to be used in electrocatalysis [119-121]. The COF constructed with precisely controlled microchannels, dopants and tunable building blocks allow for rational design of electrocatalysis. Compared with carbon and carbon nitrogen based 2D material, as well as the LDH, COF provides much higher flexibility by modifying their chemical motifs. Furthermore, the 2D COFs with their high chemical stabilities in the acids and bases conditions, and high surface areas as well as abundant active sites in their pore edges, provide the ideal material structures for efficient OER. For example, Lin et al. calculated the OER activities of some COFs supported transition metal SACs (TM-COFs). They found that the crystal field stabilization energy (CFSE) can well describe the electronic structure and OER catalytic activities of these systems [119]. Moreover, a volcano relationship between the CFSE and the OER catalytic activities on TM-COFs was established, and the Fe-COF with a minimum OER overpotential of 0.38 V is located near the peak of the volcano plot. Wannakao and co-workers theoretically studied the OER performance on metalloporphyrin (M-Por) and beta-substituted metalloporphyrins (M-Por-X, where X refers to F, Cl, and Br) in a 2D-framework, which imitate the structures of COF and MOF frameworks [122]. Their results show that there exist a scaling relationship among the adsorption free energies of the $*OH$, $*O$ and $*OOH$ intermediates. Using this scaling relationship, and the related volcano plot, Co-Por-F is identified as having the lowest OER overpotential.

In the periodic table, boron is the element at the left side of carbon, which can form at least 16 different allotropes with many promising properties. Recently, boron monolayers with high mechanical strength and metallicity have been successfully synthesized on clean Ag(111) substrates [123]. Ling presented a theoretical study on the design of β_{12} -boron monolayer (β_{12} -BM) supported single transition metal SACs (TM/ β_{12} -BM) for electrochemical OER [124]. The Ni1/ β_{12} -BM was selected as a promising electrocatalyst for OER, possessing good stabilities and is also cost-effective. Singh and co-workers theoretically studied defective borophane (BH) supported single transition metal atoms (TM-BH) as potential OER electrocatalysts [125]. Their results showed that TM-BH SACs have an increased density of states near the Fermi-level due to the coupling between the d-orbitals of the TM and the p-orbitals of surrounding B atoms. This increased density of state can enable active sites to enhance their OER performance. Additionally, Co atomically doped B vacancy BC_3 ($\text{Co}@V_B$) is found to be a promising OER electrocatalyst with an overpotential of 0.43 V. The hybridization between the 2p orbital of C and d orbital of Co indicates the strong interaction between V_B and doped Co atom [126]. The negative binding energy and positive dissolution energy properties of $\text{Co}@V_B$ suggest its high dispersibility and stability.

MXenes, as a new class of 2D layered materials, have potentials to be good electrocatalysts due to their high surface area, high electrical and thermal conductivity as well as excellent thermostability [127]. Kan and co-workers theoretically designed Nb_2CT_2 (T = O, F, and OH) anchored Pt/Pd SACs for OER [128]. Their results show that $\text{Nb}_2\text{CF}_2\text{-V}_F\text{-Pt}$ can exhibit a low OER overpotential of 0.37 V due to the electron donor capacity of the catalyst, as well as synergetic effects between the Pt atoms and the functional groups. The negative formation energy and large diffusion barrier of a single Pd/Pt atom on Nb_2CT_2 indicate high stability and dispersibility of catalysts. In addition, analysis of ELF suggests that the decorated Pt/Pd atoms on $\text{Nb}_2\text{C}(\text{OH})_2$ were attached by several H atoms of the OH groups and the strong bonding led to catalyst deactivation. Cheng et al., theoretically studied Cr_2CO_2 MXene supported Ni SAC as electrocatalyst for the OER, and found an overpotential of 0.46 V [129], the energy barrier of 4.34 eV for the relocation of the Ni atom suggests the difficult diffusion of the Ni atom along

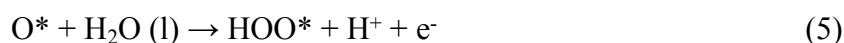
the surface. Through DFT calculations, Chen et al. investigated a series of M_2NO_2 MXenes supported SACs for OER^[130]. The calculated results show that the Cu-Ti₂NO₂ can moderately bind with the oxygenated intermediates, which makes it the most active SAC for OER with the lowest overpotential of 0.24 V. Additionally, after 5 ps AIMD simulations at 300K, they found that the Cu atoms prefer to atomically disperse rather than aggregate. Fu et al. systematically investigated the Ti₃C₂O₂ anchored 12 different transition metal atoms SACs for OER through DFT calculations^[131]. The introduction of TM atoms onto the surface of Ti₃C₂O₂ can dramatically enhance the OER performance. Due to the relatively shallow energy level of the d band center of the Pd atom in Pd₁@Ti₃C₂O₂, it results in a low OER overpotentials of 0.31 V.

4. Theory-guided rational design single-atom electrocatalysts for OER

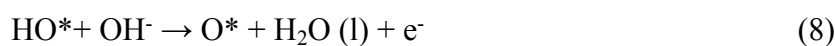
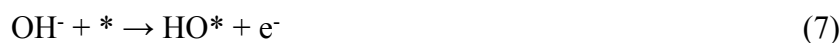
4.1 Fundamental principles of OER

In the electrochemical water-splitting, the OER is the oxidation process that occurs at the anode which produces O₂. The OER involves four-electron transfer steps, and the corresponding steps that occur under acidic and alkaline medium are described by the following equations:

Acidic medium ($2H_2O(l) \rightarrow O_2(g) + 4H^+ + 4e^-$)^[132]:



Alkaline medium ($4OH^- \rightarrow O_2(g) + 2H_2O(l) + 4e^-$)^[133]:



Where * stands for an adsorption site on the catalyst. l and g refer to liquid and gas phases, respectively. O*, HO* and HOO* refer to the three adsorbed intermediates on the active sites. The first step is the formation of HO* that adsorbed on the catalyst with

the first electron transfer. The second step is the formation of O* from HO*. The third step is the formation of HOO* from O*. The last step is the release of one O₂ molecule. Each step either takes one H₂O molecule and released one H⁺ in the acid medium, or takes one HO⁻ in the alkaline medium. The last step can go back to the first step by releasing one O₂ molecule, one electron, and one H⁺ (in the acid case) or H₂O (in the alkaline case).

The overpotential of OER (η^{OER}) on a given catalyst depends on the largest Gibbs free energies increase (ΔG) among all four steps. This bottleneck step determines the overall OER overpotential. The ΔG is calculated using the standard hydrogen electrode (SHE) as the reference for the electrode potential, where the total energy of a proton-electron pair equals to that of half of the hydrogen in the gas phase [134]. Once applied an electrode potential (U) on the OER processes (referenced from the SHE potential), the $\Delta G_U = -neU$ term should be added to the corresponding reaction free energies, where n is the number of transferred electrons in this step. The ΔG for each reaction step is thus calculated by the following equation:

$$\Delta G = \Delta E_{\text{ads}} + \Delta \text{ZPE} - T\Delta S + \Delta G_{\text{pH}} - eU \quad (9)$$

Where ΔE_{ads} refers to the adsorption energy of intermediates in each elementary reaction (equation 3-10) that can be directly obtained from DFT calculations, ΔZPE is the zero-point energy change of the frequency vibration, T is the temperature, ΔS is the change in entropy energy obtained from the frequency vibration calculation. $\Delta G_{\text{pH}} = k_{\text{B}}T \ln 10 \times \text{pH}$ can be used to consider the effect of pH value, where k_{B} is the Boltzmann constant [135, 136]. More specifically, ΔG_{pH} represents the dependence of H⁺ (or OH⁻) Gibbs free energy on the pH value, and the corresponding free energy change for this step, since each step will consume either one OH⁻ or release on H⁺.

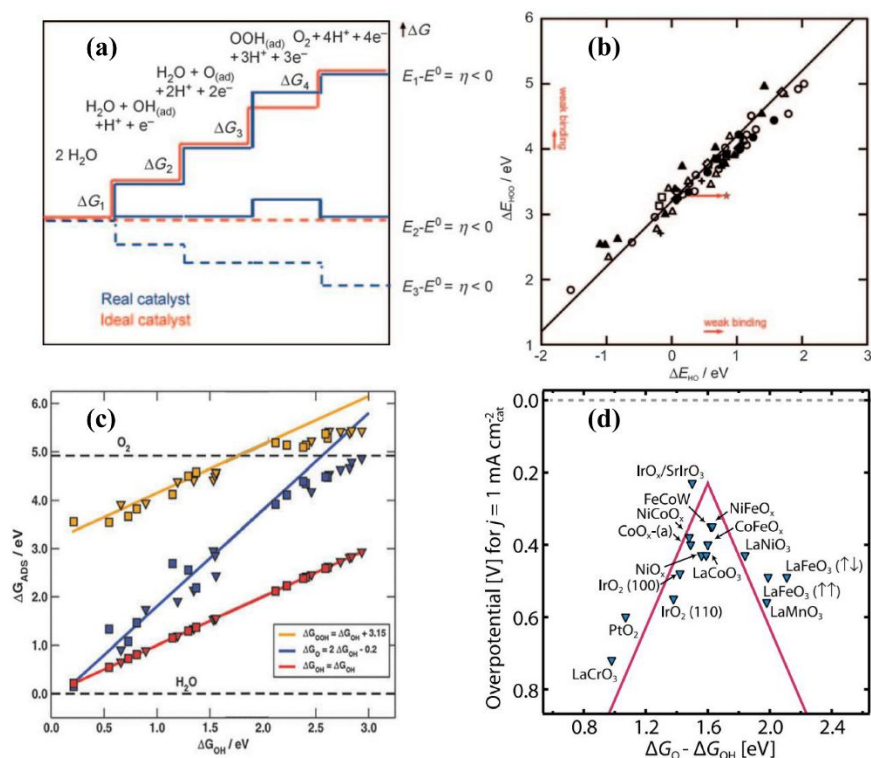


Fig. 11 (a) Gibbs free energy at $U = 0$ for the ideal and real catalysts, and (b) Adsorption energy of HOO^* plotted against the adsorption energy of HO^* on perovskites, rutiles, anatase, Mn_xO_y , Co_3O_4 , and NiO oxides. Reprinted with permission from ref. 132. Copyright 2011, Wiley-VCH Verlag GmbH & Co. KGaA, Weinheim. (c) Scaling relations among the Gibbs free energy of HO^* , O^* and HOO^* . Reprinted with permission from ref. 137. Copyright 2011, The Royal Society of Chemistry. (d) OER volcano plot for various oxides. Reprinted with permission from ref. 138. Copyright 2017, American Association for the Advancement of Science.

The overpotential of OER can be calculated by

$$\eta^{\text{OER}} = \max\{\Delta G\}/e - 1.23 \quad (10)$$

Where ΔG in Eq. (10) is calculated with $U = 0$ and $\text{pH} = 0$. As displayed in (**Fig. 11a**)^[132], for an ideal OER electrocatalyst at standard condition, all the four elemental steps with reaction free energies are the same (namely, 1.23 eV). Thus, the η^{OER} value is zero and the OER can occur at its thermodynamic limit when the four steps are equally displaced. In reality, the values of above reaction free energies are not equal, that results in a nonzero overpotential. Some rules of the overpotential can exist due to some

approximated scaling relationships among ΔG_{HO^*} , ΔG_{O^*} , and ΔG_{HOO^*} . In particular, the free energies of HOO^* and HO^* are usually linearly correlated with the slope of one and a constant intercept ($\Delta G_{\text{HOO}^*} - \Delta G_{\text{HO}^*}$) of 3.2 ± 0.2 eV that has been observed for various electrocatalyst surfaces, regardless of the type of adsorption sites, as displayed in **Fig. 11b** and **c**. The nature of this relationship stems from the fact that both adsorbed HOO^* and HO^* intermediates have a single bond between the oxygen atom and the active site catalyst atom. For the adsorbed O^* intermediate, in general, the slope between O^* and HO^* is about two due to the formation of double bonds in O^* with the electrocatalyst^[132, 137]. Based on the above scaling relationship, it can be concluded that once we obtain the calculated ΔG_{HO^*} value, then, the ΔG_{HOO^*} value can be obtained directly and *vice versa*, which can reduce the computational cost to assess the catalytic performance of a given OER electrocatalyst. Besides the above scaling relationship results in a volcano-shaped plot for the overpotential, which can be used to search for the optimal catalyst, using one descriptor to determine the whole catalyst performance. Such volcano plot also offers a straightforward way to visualize and compare the OER performance of different electrocatalysts. For example, when η^{OER} is plotted *versus* $\Delta G_{\text{O}^*} - \Delta G_{\text{HO}^*}$, a volcano-shaped plot can be obtained as exhibited in **Fig. 11d**^[132, 138]. The volcano plot and adsorbate scaling relationships can provide important information for tuning the OER catalytic performance by varying the interaction strength between the adsorbates and catalysts. This usually follows the Sabatier's principle^[139], which means too strong or too weak binding strength both leads to the adversarial effects on OER. More specifically, if the adsorption of adsorbates on the catalysts is too strong, the products will be difficult to leave and the active sites will always be occupied; if the interaction between adsorbates and catalysts is too weak, the reactants will be hard to be adsorbed at the activate site, and the reaction will be difficult to proceed. For each intermediate state in the OER, if its binding energy is too large, it will be difficult to proceed with the next step. If the binding energy is too small, this step itself is difficult to form. Therefore, how to rationally design the active sites on the catalyst to obtain moderate interaction strength between the reactant and the active site is of great importance for optimizing the OER. Theoretical calculations play a crucial role in

revealing the active sites ^[140, 141], understanding the reaction mechanisms and the structure-activity relationship for a given catalyst ^[142]. It could thus provide guidance for developing high-performance OER electrocatalysts ^[143].

4.2 Designing efficient 2D materials-based SACs for OER based on density functional theory

Volcano-shaped plot plays an important role in the rational design of efficient electrocatalysts, which reflects the Sabatier principle that the optimal catalytic performance is achieved for a given catalyst with moderate binding strength for intermediates. Trasatti reported the pioneering work on the volcano plot of the OER, who used the enthalpy of the oxide transition from the lower value to higher value for various metal oxide electrodes as a descriptor to describe the OER electrocatalytic activity ^[144]. The electrocatalytic activity of OER had then been shown to have a relationship with the oxygen adsorption Gibbs free energy (ΔG_{O^*}) ^[134, 145]. Recently, the OER activity has been related to the Gibbs free energy difference between ΔG_{HO^*} and ΔG_{HOO^*} ($\Delta G_{O^*} - \Delta G_{HO^*}$). This is a universal volcano relationship with the descriptor, which has been confirmed by various types of OER electrocatalysts, such as perovskite, metal oxides, rutiles and so on (**Fig. 11d**) ^[132]. It can be seen that the formation of HOO^* is the determining step due to the strong oxygen-adsorption that lies on the left leg of the volcano plot, while, the deprotonation of HO^* is the determining step due to the weak oxygen-adsorption that lies on the right leg of the volcano plot. Besides, for a non-ideal OER electrocatalyst, the Gibbs free energy difference between ΔG_{HO^*} and ΔG_{HOO^*} is higher than that of 2.46 eV (2×1.23 eV), as a result, the minimum theoretical η^{OER} value of 0.37 V ($[3.2 - 2.46]$ eV / $2e^-$) will be obtained. This has been confirmed in a reported experimental literature from benchmarked electrocatalysts ^[6]. Thus, by regulating the electronic properties of a catalyst to moderate the binding strength of intermediates, one can improve the OER electrocatalyst.

For the 2D materials based OER SACs, modulating the atomic structure or chemical environment around the metal active sites is considered to be an effective

strategies to optimize the interaction between intermediates and SACs. The strategies include doping various metal atoms and tuning the coordination environment of the active center as we will discuss below.

4.2.1 Doping with different metal elements. The atomically dispersed active sites can increase their utilization efficiency, and enhance the interaction strength with the support materials [146]. The doping of metal atoms can make the catalyst possess the intrinsic activity of the transition metals, and also enhance the electrical conductivity of the catalyst. Theoretical and experimental results have shown that various doped metal-active sites on a given 2D support can exhibit different electrochemical activities toward OER due to various levels of unsaturated d orbital of the transition metal atoms. For example, Zhou and co-authors screened a series of transition metal atom doped C₂N monolayer (TM@C₂N, TM = Ti, Mn, Fe, Co, Ni, Cu, Mo, Ru, Rh, Pd, Ag, Ir, Pt, and Au) as SACs for OER using DFT calculations. They found that Mn@C₂N shows the highest activity for the OER because its $\Delta G_{O^*} - \Delta G_{HO^*}$ value is the highest (1.22 eV) [115]. Qiao and co-authors experimentally found that g-C₃N₄ supported Co SAC can exhibit the highest electrochemical performance for OER with a moderate adsorption energy for the intermediate OH* [110]. Thus, by tuning the doped transition metal atom with different d orbital occupations, one support can modulate the binding strength between intermediate and catalyst to optimize the performance of OER.

4.2.2 Tuning the coordination environment of the active center. For a given metal active center, the charge redistribution caused by the different electronegativity of the coordinated atoms can affect the catalytic performance of the center transition metal atom. Therefore, changing the coordination environment of the active center atom can modulate the electronic structure of the catalyst, which provides another opportunity to tune the OER performance. To date, tuning the number and type of the coordination atoms, introducing heteroatoms around the active sites, grafting heteroatoms and functional groups on metal active center have proved to be effective ways to alter the electronic structure of the active site, and improve the performance of SACs [19, 32, 33, 147, 148]. Besides the number of coordination, the locations of the heteroatoms relative to the center metal atom, whether they are at the edge or in-plane,

can also influence the electronic properties and catalytic properties of SACs [149]. Additionally, for 2D materials, strain engineering is another a useful way to alter the interaction between the adsorbed intermediates and catalysts [150-152]. Overall, precise control of the SAC environments is of great importance to design and optimize the SAC OER catalysis.

5. Conclusions and Outlook

Electrocatalytic OER has received considerable attention due to its critical role in mass production of hydrogen as a green energy source. Significant research efforts have been devoted to design and construct high-performance and low-cost OER electrocatalysts both theoretically and experimentally. Although progress has been made for 2D materials supported SACs as OER electrocatalysts, it is still a great challenge to its design and development, especially for low-cost catalyst in practical applications. In this review, we have systematically summarized the recent progress in the strategies for experimental synthesis of SACs on various 2D supports, including the wet-chemistry method, atomic layer deposition method, high-temperature pyrolysis method, and high-temperature atomic migration and trapping method. The methods that facilitate the formation of SACs and enable researchers to tune the geometric and electronic structures have been highlighted. Furthermore, we have reviewed recent progress of SACs on various 2D supports as active OER electrocatalysts with an emphasis on the strategies of adjusting the geometric and electronic structures of SACs to improve the OER performance, such as tuning the coordination environment of the support, introducing different defects of support or second ligand on the active metal center, and strain engineering.

Despite these advances, some challenges remain in both the fundamental research and industrial application of OER electrocatalysts. First, to date, the production yield and quality of 2D materials on experiments are inadequate for large-scale applications. Consequently, it is necessary to optimize the current synthesis methods. Second, for the SACs, it is still a challenge to increase the amount of loading of the single-atoms and maintain the dispersion of active single atomic sites, making the full usage of the large

surface area of 2D materials. Additionally, the currently used metal are mainly limited in 3d transition metals (e.g. Fe, Co, and Ni). Moreover, many preparation processes are not economical enough due to expensive precursors, high-temperature treatment and complicated procedures during synthesis. Thus, more convenient, economical and scalable synthesis strategies need to be developed. Third, detecting the OER intermediates and their adsorption behavior remains a great challenge experimentally. Currently, there is no experimental tools that can effectively probe the electron transfer process, structural and electronic properties variations, and intermediate states during OER process. On the other hand, for one catalyst at a given pH and U condition, surface Pourbaix diagram reveals that the initial state of the active site before reaction might already been bounded with one or two species (e.g., O^* , H^* or HO^*). Thus, the actual OER reaction might be more complicated than the picture we provided in the above section. This makes it even more necessary to advance in situ characterization techniques, thus to capture the OER intermediates and to further understand the OER process at the atomic level. The stability of SACs has yet to be systematically studied under OER, especially at the acidic condition. The advanced characterization before- and after-OER can provide a deeper understanding of degradation mechanisms. Fourth, it is of great importance to break the adsorption Gibbs free energies scaling relationships (between HO^* , O^* , and HOO^*), in order to have better OER performance. These scaling rules limit the peak performance in the OER volcano plot, and severely limit our ability to independently tune the binding energy of different intermediate species. To fine tune the OER performance, it will be critical for being able to change the binding energies of different intermediate species independently. Fifth, the OER mechanism and the structure-activity correlation is still not entirely clear. Although theoretical calculations have been widely used to study the OER catalytic performance of many 2D SAC, the used theoretical models are relatively simple. There are many effects which have been largely ignored in many theoretical studies. These include: transition barrier at each OER step, explicit solvent effects, fixed electrode potential effect, possible multi-specie binding at the active site, salt cation or anion effect, electrolytic corrosion, charge storage at the active site, the electron transfer

nonadiabatic effect. The fixed potential effects and charge effects have already been approved to be important in 2D materials ^[153, 154], while, current DFT calculations were usually performed at constant electron numbers not constant electrode voltage. Overall, continued research efforts should be devoted to advance experimental strategies and theoretical methods, which will provide a deeper understanding of the electrocatalytic nature of OER and further guide the community in developing more efficient, stable and low-cost 2D materials SACs.

Conflicts of interest

There are no conflicts to declare.

Acknowledgements

This work is supported by the Joint Center for Artificial Photosynthesis, a DOE Energy Innovation Hub, supported through the Office of Science of the U.S. Department of Energy under Award number DE-SC0004993. We are grateful to the Chinese Scholarship Council (CSC) for providing the Ph.D. scholarship.

References

- [1] N. L. Panwar, S. C. Kaushik and S. Kothari, *Renewable Sustainable Energy Rev.*, 2011, **15**, 1513-1524.
- [2] B. C. Qiu, M. Y. Xing and J. L. Zhang, *Chem. Soc. Rev.*, 2018, **47**, 2165-2216.
- [3] J. M. Bockris, *Int. J. Hydrogen Energy.*, 2002, **27**, 731-740.
- [4] I. Dincer, *Int. J. Hydrogen Energy.*, 2012, **37**, 1954-1971.
- [5] Z. Y. Cai, X. M. Bu, P. Wang, J. C. Ho, J. H. Yang and X. Y. Wang, *J. Mater. Chem. A.*, 2019, **7**, 5069-5089.
- [6] J. H. Montoya, L. C. Seitz, P. Chakthranont, A. Vojvodic, T. F. Jaramillo and J.K. Norskov, *Nat. Mater.*, 2016, **16**, 70-81.
- [7] J. Zhang, Q. Y. Zhang and X. L. Feng, *Adv. Mater.*, 2019, 1808167.
- [8] B. M. Hunter, H. B. Gray and A. M. Muller, *Chem. Rev.*, 2016, **116**, 14120-14136.
- [9] Y. Jiao, Y. Zheng, M. Jaroniec and S. Z. Qiao, *Chem. Soc. Rev.*, 2015, **44**, 2060-2086.
- [10] M. W. Kanan and D. G. Nocera, *Science*, 2008, **321**, 1072-1075.
- [11] C. C. L. McCrory, S. Jung, J. C. Peters and T. F. Jaramillo, *J. Am. Chem. Soc.*, 2013, **135**, 16977-16987.
- [12] Y. Lee, J. Suntivich, K. J. May, E. E. Perry and Y. Shao-Horn, *J. Phys. Chem. Lett.*, 2012, **3**, 399-404.
- [13] Q. R. Shi, C. Z. Zhu, D. Du and Y. H. Lin, *Chem. Soc. Rev.*, 2019, **48**, 3181-3192.
- [14] W. T. Hong, M. Risch, K. A. Stoerzinger, A. Grimaud, J. Suntivich and Y. Shao-Horn, *Energy*

Environ. Sci., 2015, **8**, 1404-1427.

- [15] E. Antolini, *ACS Catal.*, 2014, **4**, 1426-1440.
- [16] R. Kotz, H. J. Lewerenz and S. Stucki, *J. Electrochem. Soc.*, 1983, **130**, 823-829.
- [17] R. Kotz, H. Neff and S. Stucki, *J. Electrochem. Soc.*, 1984, **131**, 72-77.
- [18] M. Hamdani, R. N. Singh and P. Chartier, *Int. J. Electrochem. Sci.*, 2010, **5**, 556-577.
- [19] D. Zhao, Z. W. Zhuang, X. Cao, C. Zhang, Q. Peng, C. Chen and Y. D. Li, *Chem. Soc. Rev.*, 2020, **49**, 2215-2264.
- [20] S. H. Sun, G. X. Zhang, N. Gauquelin, N. Chen, J. G. Zhou, S. L. Yang, W. F. Chen, X. B. Meng, D. S. Geng, M. N. Banis, R. Y. Li, S. Y. Ye, S. Knights, G. A. Botton, T. K. Sham and X. L. Sun, *Sci. Rep.*, 2013, **3**, 1775.
- [21] J. W. Su, R. X. Ge, Y. Dong, F. Hao and L. Chen, *J. Mater. Chem. A.*, 2018, **6**, 14025-14042.
- [22] J. N. Coleman, M. Lotya, A. O'Neill, S. D. Bergin, P. J. King, U. Khan, K. Young, A. Gaucher, S. De, R. J. Smith, I. V. Shvets, S. K. Arora, G. Stanton, H. Kim, K. Lee, G. T. Kim, G. S. Duesberg, T. Hallam, J. J. Boland, J. J. Wang, J. F. Donegan, J. C. Grunlan, G. Moriarty, A. Shmeliov, R. J. Nicholls, J. M. Perkins, E. M. Grieveson, K. Theuwissen, D. W. McComb, P. D. Nellist and V. Nicolosi, *Science.*, 2011, **331**, 568-571.
- [23] M. Ghidui, M. R. Lukatskaya, M. Q. Zhao, Y. Gogotsi and M. W. Barsoum, *Nature.*, 2014, **516**, 78-81.
- [24] K. S. Novoselov, A. K. Geim, S. V. Morozov, D. Jiang, Y. Zhang, S. V. Dubonos, I. V. Grigorieva and A. A. Firsov, *Science.*, 2004, **306**, 666-669.
- [25] H. Y. Jin, C. X. Guo, X. Liu, J. L. Liu, A. Vasileff, Y. Jiao, Y. Zheng and S. Z. Qiao, *Chem. Rev.*, 2018, **118**, 6337-6408.
- [26] Y. Z. Zhu, W. C. Peng, Y. Li, G. L. Zhang, F. B. Zhang and X. B. Fan, *Small Methods.*, 2019, **3**, 1800438.
- [27] B. Zhang, T. J. Fan, N. Xie, G. H. Xie and H. Zhang, *Adv. Sci.*, 2019, **6**, 1901787.
- [28] X. Zhang, A. Chen, L. T. Chen and Z. Zhou, *Adv. Energy Mater.*, 2021, 2003841.
- [29] Y. Wang, W. H. Zhang, D. H. Deng and X. H. Bao, *Chin. J. Catal.*, 2017, **38**, 1443-1453.
- [30] R. Gusmão, M. Veselý and Z. Sofer, *ACS Catal.*, 2020, **10**, 9634-9648.
- [31] S. Back, J. Lim, N. Y. Kim, Y. H. Kim and Y. Jung, *Chem. Sci.*, 2017, **8**, 1090-1096.
- [32] Q. Q. Zhang and J. Q. Guan, *J. Power Sources.*, 2020, **471**, 228446.
- [33] Y. Z. Zhu, J. Sokolowski, X. C. Song, Y. H. He, Y. Mei and G. Wu, *Adv. Energy Mater.*, 2019, **10**, 1902844.
- [34] K. Qi, M. Chhowalla and D. Voiry, *Mater. Today.*, 2020, **40**, 173-192.
- [35] S. H. Ye, F. Y. Luo, Q. L. Zhang, P. Y. Zhang, T. T. Xu, D. S. He, L. C. Guo, Y. Zhang, C. X. He, X. P. Ouyang, Q. Wang, M. Gu, J. H. Liu and X. L. Sun, *Energy Environ. Sci.*, 2019, **12**, 1000-1007.
- [36] G. X. Zhang, Y. Jia, C. Zhang, X. Y. Xiong, K. Sun, R. D. Chen, W. X. Chen, Y. Kuang, L. R. Zheng, H. L. Tang, W. Liu, J. F. Liu, X. M. Sun, W. F. Lin, H. J. Dai, *Energy Environ. Sci.*, 2019, **12**, 1317-1325.
- [37] K. Huang, L. Zhang, T. Xu, H. H. Wei, R. Y. Zhang, X. Y. Zhang, B. H. Ge, M. Lei, J. Y. Ma, L. M. Liu and H. Wu, *Nat. Commun.*, 2019, **10**, 6066.
- [38] N.T.K. Thanh, N. Maclean and S. Mahiddine, *Chem. Rev.*, 2014, **114**, 7610-7630.
- [39] M. Sleutel, J. Lutsko, A.E.S. Van Driessche, M.A. Duran-Olivencia and D. Maes, *Nat. Commun.*, 2014, **5**, 5598.

- [40] Y.N. Xia, K.D. Gilroy, H.C. Peng and X.H. Xia, *Angew. Chem. Int. Ed.*, 2017, **56**, 60-95.
- [41] H. H. Wei, K. Huang, L. Zhang, B. H. Ge, D. Wang, J. J. Lang, J. Y. Ma, D. Wang, S. Zhang, Q. Y. Li, R. Y. Zhang, N. Hussain, M. Lei, L. M. Liu and H. Wu, *Angew. Chem. Int. Ed.*, 2018, **57**, 3354-3359.
- [42] L. H. Zhang, L. L. Han, H. X. Liu, X. J. Liu and J. Luo, *Angew. Chem. Int. Ed.*, 2017, **56**, 13694-13698.
- [43] Z. R. Zhang, C. Feng, C. X. Liu, M. Zuo, L. Qin, X. P. Yan, Y. L. Xing, H. L. Li, R. Si, S. M. Zhou and J. Zeng, *Nat. Commun.*, 2020, **11**, 1215.
- [44] P. X. Liu, Y. Zhao, R. X. Qin, S. G. Mo, G. X. Chen, L. Gu, D. M. Chevrier, P. Zhang, Q. Guo, D. D. Zang, B. H. Wu, G. Fu and N. F. Zheng, *Science.*, 2016, **352**, 797-800.
- [45] C. Li, Z. Chen, H. Yi, Y. Cao, L. Du, Y. D. Hu, F. P. Kong, R. K. Campen, Y. Z. Gao, C. Y. Du, G. P. Yin, I. Y. Zhang and Y. J. Tong, *Angew. Chem. Int. Ed.*, 2020, **59**, 1-7.
- [46] P. Zhou, F. Lv, N. Li, Y. L. Zhang, Z. J. Mu, Y. H. Tang, J. P. Lai, Y. G. Chao, M. C. Luo, F. Lin, J. H. Zhou, D. Su and S. J. Guo, *Nano Energy.*, 2019, **56**, 127-137.
- [47] T. F. Li, J. J. Liu, Y. Song and F. Wang, *ACS Catal.*, 2018, **8**, 8450-8458.
- [48] Y. Q. Zhu, T. Cao, C. B. Cao, J. Luo, W. X. Chen, L. R. Zheng, J. C. Dong, J. Zhang, Y. H. Han, Z. Li, C. Chen, Q. Peng, D. S. Wang and Y. D. Li, *ACS Catal.*, 2018, **8**, 10004-10011.
- [49] J. B. Wu, H. Zhou, Q. Li, M. Chen, J. Wan, N. Zhang, L. K. Xiong, S. Li, B. Y. Xia, G. Feng, M. L. Liu and L. Huang, *Adv. Energy Mater.*, 2019, **9**, 1900149.
- [50] A. J. Han, W. X. Chen, S. L. Zhang, M. L. Zhang, Y. H. Han, J. Zhang, S. F. Ji, L. R. Zheng, Y. Wang, L. Gu, C. Chen, Q. Peng, D. S. Wang and Y. Li, *Adv Mater.*, 2018, **30**, 1706508.
- [51] Q. H. Li, W. X. Chen, H. Xiao, Y. Gong, Z. Li, L. R. Zheng, X. S. Zheng, W. S. Yan, W. C. Cheong, R. G. Shen, N. H. Fu, L. Gu, Z. B. Zhuang, C. Chen, D. S. Wang, Q. Peng, J. Li and Y. D. Li, *Adv. Mater.*, 2018, **30**, 1800588.
- [52] Y. X. Ding, A. Klyushin, X. Huang, T. Jones, D. Teschner, F. Girgsdies, T. Rodenas, R. Schlogl and S. Heumann, *Angew. Chem. Int. Ed.*, 2018, **57**, 3514-3518.
- [53] Y. Cheng, S. Y. Zhao, B. Johannessen, J. P. Veder, M. Saunders, M. R. Rowles, M. Cheng, C. Liu, M. F. Chisholm, R. D. Marco, H. M. Cheng, S. Z. Yang and S. P. Jiang, *Adv. Mater.*, 2018, **30**, 1706287.
- [54] Y. Q. Zhu, W. M. Sun, W. X. Chen, T. Cao, Y. Xiong, J. Luo, J. C. Dong, L. R. Zheng, J. Zhang, X. L. Wang, C. Chen, Q. Peng, D. S. Wang and Y. D. Li, *Adv. Funct. Mater.*, 2018, **28**, 1802167.
- [55] M. X. Chen, M. Z. Zhu, M. Zuo, S. Q. Chu, J. Zhang, Y. Wu, H. W. Liang and X. L. Feng, *Angew. Chem. Int. Ed.*, 2020, **59**, 1627-1633.
- [56] D. B. Liu, C. Q. Wu, S. M. Chen, S. Q. Ding, Y. F. Xie, C. D. Wang, T. Wang, Y. A. Haleem, Z. ur Rehman, Y. Sang, Q. Liu, X. S. Zheng, Y. Wang, B. H. Ge, H. X. Xu and L. Song, *Nano Res.*, 2018, **11**, 2217-2228.
- [57] H. L. Fei, J. C. Dong, Y. X. Feng, C. S. Allen, C. Z. Wan, B. Voloskiy, M. F. Li, Z. P. Zhao, Y. L. Wang, H. T. Sun, P. F. An, W. X. Chen, Z. Y. Guo, C. Lee, D. L. Chen, I. Shakir, M. J. Liu, T. D. Hu, Y. D. Li, A. I. Kirkland, X. F. Duan and Y. Huang, *Nat. Catal.*, 2018, **1**, 63-72.
- [58] J. Li, S. G. Chen, N. Yang, M. M. Deng, S. Ibraheem, J. H. Deng, J. Li, L. Li and Z. D. Wei, *Angew. Chem. Int. Ed.*, 2019, **58**, 7035-7039.
- [59] H. L. Fei, J. C. Dong, C. Z. Wan, Z. P. Zhao, X. Xu, Z. Y. Lin, Y. L. Wang, H. T. Liu, K. T. Zang, J. Luo, S. L. Zhao, W. Hu, W. S. Yan, I. Shakir, Y. Huang and X. F. Duan, *Adv. Mater.*, 2018, **30**, 1802146.
- [60] S. M. Xu, G. Zhong, C. J. Chen, M. Zhou, D. J. Kline, R. J. Jacob, H. Xie, S. M. He, Z. N. Huang, J. Q. Dai, A. H. Brozena, R. Shahbazian-Yassar, M. R. Zachariah, S. M. Anlage and L. B. Hu, *Matter.*,

2019, **1**, 759-769.

- [61] L. Zhao, Y. Zhang, L. B. Huang, X. Z. Liu, Q. H. Zhang, C. He, Z. Y. Wu, L. J. Zhang, J. P. Wu, W. L. Yang, L. Gu, J. S. Hu and L. J. Wan, *Nat. Commun.*, 2019, **10**, 1278.
- [62] J. Jones, H. F. Xiong, A. T. Delariva, E. J. Peterson, H. Pham, S. R. Challa, G. S. Qi, S. Oh, M. H. Wiebenga, X. I. P. Hernandez, Y. Wang and A. K. Datye, *Science*, 2016, **353**, 150-154.
- [63] C. B. Alcock and G. W. Hooper, *Proc. R. Soc. Lond. A: Math. Phys. Sci.*, 1997, **254**, 551-561.
- [64] S. J. Wei, A. Li, J. C. Liu, Z. Li, W. X. Chen, Y. Gong, Q. H. Zhang, W. C. Cheong, Y. Wang, L. R. Zheng, H. Xiao, C. Chen, D. S. Wang, Q. Peng, L. Gu, X. D. Han, J. Li and Y. D. Li, *Nat. Nanotechnol.*, 2018, **13**, 856-861.
- [65] Y. G. Wang, D. H. Mei, V. A. Glezakou, J. Li and R. Rousseau, *Nat. Commun.*, 2015, **6**, 6511.
- [66] Y. T. Qu, B. X. Chen, Z. J. Li, X. Z. Duan, L. G. Wang, Y. Lin, T. W. Yuan, F. Y. Zhou, Y. D. Hu, Z. K. Yang, C. M. Zhao, J. Wang, C. Zhao, Y. M. Hu, G. Wu, Q. H. Zhang, Q. Xu, B. Y. Liu, P. Gao, R. You, W. X. Huang, L. R. Zheng, L. Gu, Y. E. Wu and Y. D. Li, *J. Am. Chem. Soc.*, 2019, **141**, 4505-4509.
- [67] J. C. Liu, Y. G. Wang and J. Li, *J. Am. Chem. Soc.*, 2017, **139**, 6190-6199.
- [68] J. C. Liu, Y. Tang, Y. G. Wang, T. Zhang and J. Li, *Natl. Sci. Rev.*, 2018, **5**, 638-641.
- [69] R. Lang, W. Xi, J. C. Liu, Y. T. Cui, T. B. Li, A. F. Lee, F. Chen, Y. Chen, L. Li, L. Li, J. Lin, S. Miao, X. Y. Liu, A. Q. Wang, X. D. Wang, J. Luo, B. T. Qiao, J. Li and T. Zhang, *Nat. Commun.*, 2019, **10**, 234.
- [70] Y. T. Qu, Z. J. Li, W. X. Chen, Y. Lin, T. W. Yuan, Z. K. Yang, C. M. Zhao, J. Wang, C. Zhao, X. Wang, F. Y. Zhou, Z. B. Zhuang, Y. E. Wu and Y. D. Li, *Nat. Catal.*, 2018, **1**, 781-786.
- [71] Z. Q. Zhang, Y. G. Chen, L. Q. Zhou, C. Chen, Z. Han, B. S. Zhang, Q. Wu, L. J. Yang, L. Y. Du, Y. F. Bu, P. Wang, X. Z. Wang, H. Yang and Z. Hu, *Nat. Commun.*, 2019, **10**, 1657.
- [72] J. K. Li, L. Jiao, E. Wegener, L. L. Richard, E. S. Liu, A. Zitolo, M. T. Sougrati, S. Mukerjee, Z. P. Zhao, Y. Huang, F. Yang, S. C. Zhong, H. Xu, A. J. Kropf, F. Jaouen, D. J. Myers and Q. Y. Jia, *J. Am. Chem. Soc.*, 2020, **142**, 1417-1423.
- [73] D. X. Yan, J. Chen and H. P. Jia, *Angew. Chem. Int. Ed.*, 2020, **59**, 1-7.
- [74] H. Zhou, Y. F. Zhao, J. Xu, H. R. Sun, Z. J. Li, W. Liu, T. W. Yuan, W. Liu, X. Q. Wang, W. C. Cheong, Z. Y. Wang, X. Wang, C. Zhao, Y. C. Yao, W. Y. Wang, F. Y. Zhou, M. Chen, B. J. Jin, R. B. Sun, J. Liu, X. Hong, T. Yao, S. Q. Wei, J. Luo and Y. E. Wu, *Nat. Commun.*, 2020, **11**, 335.
- [75] Q. Fan, P. F. Hou, C. Choi, T. S. Wu, S. Hong, F. Li, Y. L. Soo, P. Kang, Y. S. Jung and Z. Y. Sun, *Adv. Energy Mater.*, 2019, **10**, 1903068.
- [76] H. Y. Jin, S. Sultan, M. R. Ha, J. N. Tiwari, M. G. Kim and K. S. Kim, *Adv. Funct. Mater.*, 2020, **30**, 2000531.
- [77] Y. T. Qu, L. G. Wang, Z. J. Li, P. Li, Q. H. Zhang, Y. Lin, F. Y. Zhou, H. J. Wang, Z. K. Yang, Y. D. Hu, M. Z. Zhu, X. Y. Zhao, X. Han, C. M. Wang, Q. Xu, L. Gu, J. Luo, L. R. Zheng and Y. E. Wu, *Adv. Mater.*, 2019, **31**, 1904496.
- [78] W. J. Tang, J. Li, J. Zheng, W. Chu and N. Wang, *Chem. Commun.*, 2020, **56**, 9198-9201.
- [79] J. Li, Y. N. Zhou, W. J. Tang, J. Zheng, X. P. Gao, N. Wang, X. Chen, M. Wei, X. Xiao and W. Chu, *Appl. Catal. B.*, 2021, **285**, 119861.
- [80] Z. Y. Luo, Y. X. Ouyang, H. Zhang, M. L. Xiao, J. J. Ge, Z. Jiang, J. L. Wang, D. M. Tang, X. Z. Cao, C. P. Liu and W. Xing, *Nat. Commun.*, 2018, **9**, 2120.
- [81] Y. Y. Feng, Y. X. Guan, H. J. Zhang, Z. Y. Huang, J. Li, Z. Q. Jiang, X. Gu and Y. Wang, *J. Mater. Chem. A*, 2018, **6**, 11783-11789.

- [82] Y. N. Chen, X. Zhang and Z. Zhou, *Small Methods.*, 2019, **3**, 1900050.
- [83] L. Z. Zhang, Y. Jia, G. P. Gao, X. C. Yan, N. Chen, J. Chen, M. T. Soo, B. Wood, D. J. Yang, A. J. Du and X. D. Yao, *Chem.*, 2018, **4**, 285-297.
- [84] Y. G. Li, Z. S. Wu, P. F. Lu, X. Wang, W. Liu, Z. B. Liu, J. Y. Ma, W. C. Ren, Z. Jiang and X. H. Bao, *Adv. Sci.*, 2020, **7**, 1903089.
- [85] Y. Q. Xu, W. F. Zhang, Y. G. Li, P. F. Lu and Z. S. Wu, *J. Energy Chem.*, 2020, **43**, 52-57.
- [86] Y. N. Zhou, G. P. Gao, Y. Li, W. Chu and L. W. Wang, *Phys. Chem. Chem. Phys.*, 2019, **21**, 3024-3032.
- [87] P. Z. Chen, T. P. Zhou, L. L. Xing, K. Xu, Y. Tong, H. Xie, L. D. Zhang, W. S. Yan, W. S. Chu, C. Z. Wu and Y. Xie, *Angew. Chem. Int. Ed.*, 2017, **56**, 610-614.
- [88] Y. Q. Xu, W. F. Zhang, Y. G. Li, P. F. Lu, Y. Wang and Z. S. Wu, *Front. Mater.*, 2019, **6**, 271.
- [89] G. X. Li, Y. L. Li, H. B. Liu, Y. B. Guo, Y. J. Li and D. B. Zhu, *Chem. Commun.*, 2010, **46**, 3256-3258.
- [90] H. D. Yu, L. Hui, Y. R. Xue, Y. X. Liu, Y. Fang, C. Y. Xing, C. Zhang, D. Y. Zhang, X. Chen, Y. C. Du, Z. Q. Wang, Y. Gao, B. L. Huang and Y. L. Li, *Nano Energy.*, 2020, **72**, 104667.
- [91] T. W. He, S. K. Matta, G. Will and A. J. Du, *Small Methods.*, 2019, 1800419.
- [92] X. P. Gao, Y. N. Zhou, Y. J. Tan, S. Q. Liu, Z. W. Cheng and Z. M. Shen, *Appl. Surf. Sci.*, 2019, **492**, 8-15.
- [93] X. P. Gao, Y. N. Zhou, S. Q. Liu, Z. W. Cheng, Y. J. Tan and Z. M. Shen, *Appl. Surf. Sci.*, 2020, **502**, 144155.
- [94] X. P. Gao, Y. N. Zhou, Y. J. Tan, S. Q. Liu, Z. W. Cheng and Z. M. Shen, *Phys. Chem. Chem. Phys.*, 2020, **22**, 2457-2465.
- [95] X. P. Gao, L. Mei, Y. N. Zhou and Z. M. Shen, *Nanoscale.*, 2020, **12**, 7814-7821.
- [96] L. Lv, Z. Y. Yang, K. Chen, C. D. Wang and Y. J. Xiong, *Adv. Energy Mater.*, 2019, **9**, 1803358.
- [97] F. Song and X. L. Hu, *J. Am. Chem. Soc.*, 2014, **136**, 16481-16484.
- [98] Y. Kong, J. Li, Y. Wang, W. Chu and Z. Q. Liu, *Catal. Lett.*, 2020, **150**, 3049-3057.
- [99] H. F. Liang, F. Meng, M. Caban-Acevedo, L. S. Li, A. Forticaux, L. C. Xiu, Z. C. Wang and S. Jin, *Nano Lett.*, 2015, **15**, 1421-1427.
- [100] M. Wei, J. Li, W. Chu and N. Wang, *J. Energy Chem.*, 2019, **38**, 26-33.
- [101] Y. Y. Wang, Y. Q. Zhang, Z. J. Liu, C. Xie, S. Feng, D. D. Liu, M. F. Shao and S. Y. Wang, *Angew. Chem. Int. Ed.*, 2017, **56**, 5867-5871.
- [102] Y. Y. Wang, C. Xie, Z. Y. Zhang, D. D. Liu, R. Chen and S. Y. Wang, *Adv. Funct. Mater.*, 2018, **28**, 1703363.
- [103] M. K. Cai, Q. L. Liu, Z. Q. Xue, Y. L. Li, Y. N. Fan, A. P. Huang, M. R. Li, M. Croft, T. A. Tyson, Z. F. Ke and G. Q. Li, *J. Mater. Chem. A.*, 2020, **8**, 190-195.
- [104] J. F. Zhang, J. Y. Liu, L. F. Xi, Y. Y. Yu, N. Chen, S. H. Sun, W. C. Wang, K. M. Lange and B. Zhang, *J. Am. Chem. Soc.*, 2018, **140**, 3876-3879.
- [105] P. S. Li, M. Y. Wang, X. X. Duan, L. R. Zheng, X. P. Cheng, Y. F. Zhang, Y. Kuang, Y. P. Li, Q. Ma, Z. X. Feng, W. Liu and X. M. Sun, *Nat. Commun.*, 2019, **10**, 1711.
- [106] D. Y. Chung, P. P. Lopes, P. F. B. D. Martins, H. Y. He, T. Kawaguchi, P. Zapol, H. You, D. Tripkovic, D. Strmcnik, Y. S. Zhu, S. Seifert, S. Lee, V. R. Stamenkovic and N. M. Markovic, *Nat. Energy.*, 2020, **5**, 222-230.
- [107] C. L. Dong, X. L. Zhang, J. Xu, R. Si, J. Sheng, J. Luo, S. N. Zhang, W. J. Dong, G. B. Li, W. C. Wang and F. Q. Huang, *Small.*, 2020, **16**, 1905328.

- [108] Y. K. Zhang, C. Q. Wu, H. L. Jiang, Y. X. Lin, H. J. Liu, Q. He, S. M. Chen, T. Duan and L. Song, *Adv. Mater.*, 2018, **30**, 1707522.
- [109] J. Q. Yan, L. Q. Kong, Y. J. Ji, J. White, Y. Y. Li, J. Zhang, P. F. An, S. Z. Liu, S. T. Lee and T. Y. Ma, *Nat. Commun.*, 2019, **10**, 2149.
- [110] Y. Zheng, Y. Jiao, Y. H. Zhu, Q. R. Cai, A. Vasileff, L. H. Li, Y. Han, Y. Chen and S. Z. Qiao, *J. Am. Chem. Soc.*, 2017, **139**, 3336-3339.
- [111] L. Y. Liu, H. Su, F. M. Tang, X. Zhao and Q. H. Liu, *Nano Energy*, 2018, **46**, 110-116.
- [112] L. L. Cao, Q. Q. Luo, J. J. Chen, L. Wang, Y. Lin, H. J. Wang, X. K. Liu, X. Y. Shen, W. Zhang, W. Liu, Z. M. Qi, Z. Jiang, J. L. Yang and T. Yao, *Nat. Commun.*, 2019, **10**, 4849.
- [113] D. B. Liu, S. Q. Ding, C. Q. Wu, W. Gan, C. D. Wang, D. F. Cao, Z. u. Rehman, Y. Sang, S. M. Chen, X. S. Zheng, Y. Wang, B. H. Ge and L. Song, Synergistic effect of an atomically dual-metal doped catalyst for highly efficient oxygen evolution, *J. Mater. Chem. A.*, 2018, **6**, 6840-6846.
- [114] X. Y. Li, P. Cui, W. H. Zhong, J. Li, X. J. Wang, Z. W. Wang and J. Jiang, *Chem. Commun.*, 2016, **52**, 13233-13236.
- [115] X. Zhang, A. Chen, Z. H. Zhang, M. G. Jiao and Z. Zhou, *J. Mater. Chem. A.*, 2018, **6**, 11446-11452.
- [116] Y. N. Zhou, G. P. Gao, J. Kang, W. Chu and L. W. Wang, *J. Mater. Chem. A.*, 2019, **7**, 12050-12059.
- [117] Y. N. Zhou, G. P. Gao, J. Kang, W. Chu and L. W. Wang, *Nanoscale*, 2019, **11**, 18169-18175.
- [118] Y. N. Zhou, G. P. Gao, W. Chu and L. W. Wang, *Nanoscale Adv.*, 2020, **2**, 710-716.
- [119] C. Y. Lin, L. P. Zhang, Z. H. Zhao and Z. H. Xia, *Adv. Mater.*, 2017, **29**, 1606635.
- [120] X. Cui, S. Lei, A. C. Wang, L. K. Gao, Q. Zhang, Y. K. Yang and Z. Q. Lin, *Nano Energy*, 2020, **70**, 104525.
- [121] P. Peng, L. Shi, F. Huo, C. X. Mi, X. H. Wu, S. J. Zhang and Z. H. Xiang, *Sci. Adv.*, 2019, **5**, 2322.
- [122] S. Wannakao, T. Maihom, K. Kongpatpanich, J. Limtrakul and V. Promarak, *Phys. Chem. Chem. Phys.*, 2017, **19**, 29540-29548.
- [123] A. J. Mannix, X. F. Zhou, B. Kiraly, J. D. Wood, D. Alducin, B. D. Myers, X. L. Liu, B. L. Fisher, U. Santiago, J. R. Guest, M. J. Yacaman, A. Ponce, A. R. Oganov, M. C. Hersam and N.P. Guisinger, *Science*, 2015, **350**, 1513-1516.
- [124] C. Y. Ling, L. Shi, Y. X. Ouyang, X. C. Zeng and J. L. Wang, *Nano Lett.*, 2017, **17**, 5133-5139.
- [125] Y. Singh, S. Back and Y. Jung, *Phys. Chem. Chem. Phys.*, 2018, **20**, 21095-21104.
- [126] Y. N. Zhou, G. P. Gao, W. Chu and L. W. Wang, *Nanoscale*, 2021, **13**, 1331-1339.
- [127] N. K. Chaudhari, H. Jin, B. Kim, D. S. Baek, S. H. Joo and K. Lee, *J. Mater. Chem. A.*, 2017, **5**, 24564-24579.
- [128] D. X. Kan, D. S. Wang, X. L. Zhang, R. Q. Lian, J. Xu, G. Chen and Y. J. Wei, *J. Mater. Chem. A.*, 2020, **8**, 3097-3108.
- [129] Y. W. Cheng, J. H. Dai, Y. Song and Y. M. Zhang, *ACS Appl. Energy Mater.*, 2019, **2**, 6851-6859.
- [130] Z. G. Chen, X. L. Fan, Z. H. Shen, X. P. Ruan, L. Wang, H. H. Zeng, J. H. Wang, Y. R. An and Y. Hu, *ChemCatChem*, 2020, **12**, 4059-4066.
- [131] Z. Z. Fu, C. Y. Ling and J. L. Wang, *J. Mater. Chem. A.*, 2020, **8**, 7801-7807.
- [132] I. C. Man, H. Y. Su, F. Calle-Vallejo, H. A. Hansen, J. I. Martínez, N. G. Inoglu, J. Kitchin, T. F. Jaramillo, J. K. Nørskov and J. Rossmeisl, *ChemCatChem*, 2011, **3**, 1159-1165.
- [133] N. T. Suen, S. F. Hung, Q. Quan, N. Zhang, Y. J. Xu and H. M. Chen, *Chem. Soc. Rev.*, 2017, **46**, 337.

- [134] J. Rossmeisl, A. Logadottir and J. K. Nørskov, *Chem. Phys.*, 2005, **319**, 178-184.
- [135] J. K. Nørskov, J. Rossmeisl, A. Logadottir and L. Lindqvist, *J. Phys. Chem. B.*, 2004, **108**, 17886-17892.
- [136] A. A. Peterson, F. Abild-Pedersen, F. Studt, J. Rossmeisl and J. K. Nørskov, *Energy Environ. Sci.*, 2010, **3**, 1311-1315.
- [137] F. Calle-Vallejo, J. I. Martinez and J. Rossmeisl, *Phys. Chem. Chem. Phys.*, 2011, **13**, 15639-15643.
- [138] Z. W. Seh, J. Kibsgaard, C. F. Dickens, I. Chorkendorff, J. K. Nørskov and T. F. Jaramillo, *Science.*, 2017, **355**, 6321.
- [139] J. K. Nørskov, T. Bligaard, A. Logadottir, J. R. Kitchin, J. G. Chen, S. Pandalov and U. Stimming, *J. Electrochem. Soc.*, 2005, **152**, 23-26.
- [140] J. Liang, Y. Jiao, M. Jaroniec and S. Z. Qiao, *Angew. Chem. Int. Ed.*, 2012, **51**, 11496-11500.
- [141] L. P. Zhang, J. B. Niu, L. M. Dai and Z. H. Xia, *Langmuir.*, 2012, **28**, 7542-7550.
- [142] E. Skulason, G. S. Karlberg, J. Rossmeisl, T. Bligaard, J. Greeley, H. Jonsson and J. K. Nørskov, *Phys. Chem. Chem. Phys.*, 2007, **9**, 3241-3250.
- [143] J. K. Nørskov, T. Bligaard, J. Rossmeisl and C. H. Christensen, *Nat. Chem.*, 2009, **1**, 37-46.
- [144] S. Trasatti, *Electrochim. Acta.*, 1984, **29**, 1503-1512.
- [145] J. Rossmeisl, Z. W. Qu, H. Zhu, G. J. Kroes and J. K. Nørskov, *J. Electroanal. Chem.*, 2007, **607**, 83-89.
- [146] X. F. Yang, A. Q. Wang, B. T. Qiao, J. Li, J. Y. Liu and T. Zhang, *Acc. Chem. Res.*, 2013, **46**, 1740-1748.
- [147] C. Z. Zhu, Q. R. Shi, S. Feng, D. Du and Y. H. Lin, *ACS Energy Lett.*, 2018, **3**, 1713-1721.
- [148] L. Tang, X. G. Meng, D. H. Deng and X. H. Bao, *Adv. Mater.*, 2019, 1901996.
- [149] C. T. Chen, G. L. Chen and X. K. Kong, *Inorg. Chem.*, 2018, **57**, 13020-13026.
- [150] G. P. Gao, Y. Jiao, F. X. Ma, Y. L. Jiao, E. Waclawik and A. J. Du, *J. Catal.*, 2015, **332**, 149-155.
- [151] G. P. Gao, Q. Sun and A. J. Du, *J. Phys. Chem. C.*, 2016, **120**, 16761-16766.
- [152] B. S. Sa, Y. L. Li, J. S. Qi, R. Ahuja and Z. M. Sun, *J. Phys. Chem. C.*, 2014, **118**, 26560-26568.
- [153] D. Kim, J. J. Shi and Y. Y. Liu, *J. Am. Chem. Soc.*, 2018, **140**, 9127-9131.
- [154] G. P. Gao and L. W. Wang, *J. Catal.*, 2020, **391**, 530-538.